Diploma Thesis

Investigation on cement slurries infiltration for the manufacturing of light weight concrete

submitted in satisfaction of the requirements for the degree
Diplom-Ingenieur
of the TU Wien, Faculty of Civil and Environmental Engineering

---

Diplomarbeit

Untersuchung zur Infiltration von Zementschlämmen für die Herstellung von Leichtbeton

ausgeführt zum Zwecke der Erlangung des akademischen Grads
Diplom-Ingenieur
eingereicht an der TU Wien, Fakultät für Bau- und Umweltingenieurwesen

Bernhard Stuchlik, BSc

Matr.Nr.: 01607482

Betreuung: Univ.Prof. **Agathe Robisson**, PhD
Ass. Prof. Dr. **Teresa Liberto**, BSc MSc
Dipl.-Ing. Dr.techn **Johannes Kirnbauer**
Institut für Institut für Werkstofftechnologie, Bauphysik und Bauökologie
Forschungsbereich Baustofflehre, Werkstofftechnologie
Technische Universität Wien
Karlsplatz 13/E207-01, 1040 Wien, Österreich

Wien, im November 2023 _____

Kurzfassung

Unsere Studie konzentriert sich auf die Analyse der Infiltration eines Zementleims in ein körniges Gerüst aus Blähtonkügelchen, bekannt als Leca. Ziel der Arbeit ist es, eine Mischung und ein Herstellungsverfahren zu entwickeln, die im Vergleich zu herkömmlichem Beton ein geringeres Gewicht, gute thermische Eigenschaften und Beständigkeit aufweist. Wir standen vor experimentellen Herausforderungen wie der Porosität der Leca-Kugeln und ihrer Wasseraufnahme sowie der Zusammensetzung des Zementleims mit verschiedenen Zusatzmitteln und der Packungsdichte des Korngerüsts. Um dies zu untersuchen, haben wir eine Versuchsanordnung entwickelt, bei der wir die Zementsuspension durch ein mit Leca gefülltes Rohr von unten nach oben gepumpt haben. Es wurden mehrere umfassende Tests durchgeführt, wobei bei jeder Iteration geringfügige Änderungen vorgenommen wurden, um die strukturelle Integrität des Versuchsaufbaus gegenüber dem während des Pumpvorgangs erzeugten Drücken und den ausgeübten Kräften zu gewährleisten. Wir untersuchten Parameter wie die Leca-Perlengröße, die Wassersättigung, den Wasser-Zement-Wert, den Dichtetest, die Wärmeleitfähigkeit und die rheologischen Eigenschaften des Zementschlamms, um die für eine erfolgreiche Infiltration erforderlichen Eigenschaften besser zu verstehen. Die zusätzliche Untersuchung des Zementleimes, insbesondere die Verwendung einer LC^3-Mischung, führt zu einer weiteren positiven Entwicklung in diesem Versuch, da diese Mischung eine geringere CO_2-Belastung aufweist.. Durch Variation des Wasser-Zement-Wertes, des PCE-Gehaltes, der Zusatzmittel und der Additive ist es möglich, einen Zementstein mit geringerer Entmischung und höherer Packungsdichte und damit verbesserter Fähigkeit zum Eindringen in die Hohlräume sowohl zwischen der Matrix als auch in die Oberflächenporen der Perlen zu erzielen. Eine Reduzierung des Wasser-Zement-Wertes und eine Erhöhung des PCE-Gehaltes sowie die zusätzliche Verwendung von Metakaolin und Mikrosilika waren hilfreich.

Abstract

Our study focuses on the analysis of the infiltration of a cement paste into a granular framework of expanded clay beads known as Leca. The aim of the work is to develop a mixture and a manufacturing process that have lower weight, good thermal properties and resistance compared to conventional concrete. We faced experimental challenges such as the porosity of the leca spheres and their water absorption, as well as the composition of the cement paste with different admixtures and the packing density of the grain skeleton. To investigate this, we have developed a set-up in which we pump the cement slurry through a pipe filled with Leca from the bottom to the top. Multiple comprehensive tests were conducted, incorporating slight modifications during each iteration, with the overarching goal of guaranteeing the structural integrity of the experimental setup against the pressures generated and the forces exerted during the pumping process. We examined parameters such as the Leca bead size, water saturation, water-cement ratio, density test, thermal conductivity and rheological properties of the cement slurry to better understand the properties required for successful infiltration. The additional investigation of the cement paste, especially the use of a LC^3 mixture, could lead to a further positive development in this experiment, due to a lower CO_2 load induced by this mixture. By varying the water-cement ratio, PCE content, admixtures, and additives, it is possible to achieve a cement paste with lower segregation and a higher packing density and thus improved ability to penetrate into the voids both between the matrix and into surface pores of the beads. A reduction of the water-cement ratio and an increase of the PCE content as well as the additional use of metakaolin and microsilica were helpful.

Contents

Introduction

Concrete is a foundational construction material, typically composed of aggregates, cement, and water. Lightweight concrete, as an alternative type, incorporates lightweight aggregates to reduced bulk density [9]. In lightweight concrete, the cement matrix assumes the load-bearing role, and lightweight aggregates contribute to structural integrity [21]. Due to its simplicity, lightweight concrete finds application in various construction elements such as walls, basements, ceilings, and slender load-bearing components like bridge beams. In this study, we investigate the infiltration and behavior of expanded clay beads, commonly used in lightweight concrete.

Our study focuses on the analysis of the infiltration process of a cement paste into a pack of lightweight aggregates comprising expanded clay beads. This infiltration process presents several intricate challenges. Firstly, cement paste is a dense suspension that consists of water and approximately 45% by volume of 10-micron-sized particles, and it exhibits a significant yield stress. Secondly, the paste must navigate a complex path as it traverses through the densely packed beads. Thirdly, these beads themselves are porous, and when not pre-saturated with water, they tend to draw water from the cement paste, giving rise to filtration issues that can ultimately hinder the pumping process.

To explore these complex systems, we established an experimental setup in which a cement paste is pumped from from lower to the upper section through a pipe filled with clay beads. This setup incorporates a pressure sensor situated at the base of the pipe, where the beads are located, enabling precise pressure measurements.

We explored several parameters that influence the pumping efficiency, including the bead size range, pre-saturation of the beads with water, and the water-to-cement ratio of the paste. Additionally, we conducted tests to evaluate the rheological characteristics of the cement slurry, as well as the density and thermal conductivity of the solidified concrete.

Furthermore, we used mixtures of limestone calcined clay cement (LC^3) and examined the influence of different particle shapes, ranging from spherical to platelet, on the procress. We also manipulated the rheological properties of the paste by adjusting the formulation, including variations in the water-to-cement ratio, superplasticizer content, particle size distribution of solid additives, and admixtures. These adjustments were aimed at formulating a mixture with reduced segregation and filtration tendencies, ultimately enhancing its capacity for efficient pumping through the bed of beads. Infiltration of Leca beads has proven to be exceedingly challenging, particularly for beads below 3 mm, as it necessitates high pumping pressure and currently results in water still being expelled from the slurry, causing clogging. The compressive strength in the successfully executed infiltration tests is only about one-third of that of conventional concrete, such as C25/30, highlighting the imperative need for further research in this domain. Nonetheless, the outcomes of this study will serve as a valuable resource to guide future research strategies and supply essential data for the advancement of investigations into the infiltration of slurries into Leca beads. This study is divided into several chapters, each of which addresses pivotal aspects of the research:

In **Chapter 1, State of the Art**, we provide essential background information relevant to the thesis, including an overview of LC3 properties, moisture states of grains, thermal conductivity,

and packing density. This knowledge serves as a foundation for interpreting the subsequent results.

In **Chapter 2, Materials and Methods**, we describes in detail the materials used and the methods employed. It includes the mixing protocol, the experimental setup and the different tests performed to investigate the subject.

In **Chapter 3, Results and Discussion**, the results of this study are presented. We used two different slurry compositions, each with three different grain sizes, and discuss their effects to provide a comprehensive analysis of the results.

In **Chapter 4, Conclusion**, we summarizes our key findings from the research.

In the **Appendix**, there is information about initial failed tests and preliminary tests that were conducted prior to the working set up. These findings shed light on the process that led to our final results.

Chapter 1

State of the art

Lightweight concrete is defined in accordance with DIN EN 206-1[11] as concrete with a bulk density ranging from 800 to 2000 kg/m³, whereas conventional concrete possesses a bulk density of 2000 to 2600 kg/m³. In contrast, ultra-lightweight concrete (LWC), has a bulk density of about 350 kg/m³ and utilizes lightweight aggregates with high porosity. These aggregates contain up to 85% air pores per unit volume, accounting for not only the reduce weight but also the diminished thermal conductivity of the concrete [21, 35]. The construction industry plays a significant role in addressing climate change by developing enviromentally freindly and sustainable solutions. Energy consumption in construction has a substantial yet often disregarded impact on global energy use [15].

The European Union has set the ambitious goal of achieving climate neutral by 2050. To align with the objectives of the Paris Agreement, it is imperative for the construction industry to make substantial reductions in its energy consumption. A report by the European Academies Science Advisory Council (EASAC) [13], attributing 25% of Europe's greenhouse gas emissions to the energy consumption of buildings. Consequently, the construction sector is urged to take immediate and planned action, whether in the context of renovations or new construction projects.

The sustainability of buildings, particularly concerning energy consumption for heating and cooling, is progressively gaining importance [13]. Lightweight concrete emerges as a construction material offering numerous advantages. Its most notable benefit, when compared to standard concrete, is its substantial reduction in weight. Lightweight concrete, with a density ranging from 800-1000 kg/m³ is significantly lighter than conventional concrete (approx. 2500 kg/m³) [15]. This reduction in weight proves invaluable as it diminishes structural loads, simplifies handling and transportation, resulting in cost savings, and enhances the efficiency of construction process. Another prominent advantage is its versatility. Lightweight concrete finds application in a wide spectrum of architectural structures, ranging from residential buildings to bridges and industrial facilities. This versatility allows for architectural diversity. Moreover, the porous nature of the concrete, with air entrapment as a consequence, grants excellent thermal insulation properties. This enhance the energy efficiency of LWC, subsequently reducing building costs. Importantly, despite its low weight, LWC exhibits good stability and durability [15]. Notably, the production of lightweight concrete entails lower consumption of raw materials and reduced energy usage, contributing to a diminished ecological footprint. Furthermore, the thermal insulation property of LWC adds to its environmental friendliness [15]. As illustrated in figure 1.1, this type of concrete is ideally suited for construction without the need for additional insulation. It effectively maintain stable interior temperatures removing the requirement for materials such as rigid foam insulation panels, which are commonly employed in modern construction but are less environmentally friendly.

LWC is employed in a variety of applications where the benefits of good thermal insulation and reduced weight are essential. There are various types of lightweight concrete, including:

- Structural (compacted) lightweight concrete

- Aggregate lightweight concrete
- Foam concrete
- Aerated concrete

The selection of specific types of lightweight concrete in construction is determined by the needs of each project. The dry bulk density of lightweight concrete impacts its mechanical properties and thermal conductivity. Consequently, the use of Lightweight Concrete (LWC) represents a significant advancement in the construction industry, enabling a broad spectrum of innovative solutions [44]. We strive to develop concrete with minimal weight, good thermal properties and at the same time high strength in order to combine the advantages of lightweight concrete with a robust resistance that comes close to that of conventional concrete. In order to use the advantages of lightweight concrete and still achieve a higher load-bearing capacity, we are investigating the infiltration of a structure of Leca to obtain an improved load-bearing structure. Both the packing density and the appropriate slurry will be investigated and adjusted to ensure this goal.

Fig. 1.1: Liapor Referenzobjekt Kirche Pilzehausen [23].

1.1 Lab-rheology

Rheology is the study of the flow and deformation characterisitics of materials [6]. Typically, rheological behavior is measured by applying a controlled deformation or strain to a material over a specified duration and recording the resulting force response, or conversely, by applying a controlled force and monitoring the resulting deformation. This approach allows the determination of the fresh properties of dense suspensions, including parameters such as viscosity, yield stress and viscoelastic behavior. Various test methods are available for measuring rheological properties, encompassing rheometer tests and laboratory rheology tests, such as cone spread and funnel tests for the measurement of rheological properties [6, 17, 18].

In our study, we conducted laboratory rheology tests, with a primary focus on determining the critical parameter known as the "yield stress". Yield-stress fluids are materials that exhibit solid-like behaviour up to a certain shear stress, displaying only elastic deformation [25]. It is only when this shear stress threshold is exceeded that the material and undergoes irreversible deformation. This transition is refered to as the yield point. To simplify, the yield point can be defined as the minimum stress required to induce flow in a material, and cementitious materials fall within the category of yield-stress fluids. We differentiate between two key types of yield points:

1. Dynamic Yield Point: This represents the minimum stress necessary to maintain the continuous flow of the material.

2. Static Yield Point: This is the stress level required to initiate the flow process, marking the transition from solid-like to fluid-like behavior in the material.

Understanding and quantifying the yield stress is critical in the assessment of materials like cementitious substances, as it is a fundamental parameter governing their flow behavior and deformation characteristics.

We estimate the yield stress using a test known as the Hägermann-Konus test [12] (see sec. 2.2.4). This involves measuring the spread (radius) and applying equation 1.1.

$$\tau_0 = \frac{225 \rho g V^2}{128 \pi^2 R^2} \tag{1.1}$$

with:

τ_0	yield stress [Pa]
ρ	density $[kg/m^3]$
V	Volume of cone $[m^3]$
g	gravity $[m/s^2]$
R	Radius of spread [m]

1.2 Packing Density

The packing density of a granular material is directly related to the ratio of solids to total volume. In concrete construction, this concept is of great importance to achieve a high aggregate packing density. This is critical to creating an efficient structure with less reliance on cement paste, as higher packing density increases surface contact between the aggregates, allowing more direct transfer of compressive forces directly through the aggregates [37, 45].

The packing density, denoted as "D," represents the proportion of solid volume relative to the total volume of a particle bed and can be calculated using the formula:

$$D = 1 - \frac{\varepsilon}{100}$$

The formula explicitly quantifies the relationship between solid volume and the void content within the particle bed.

In the discussion of packing density, it is important to account for the influence of the wall. This phenomenon alters the distribution of particle near walls, and amplifies the presence of voids in regions near surfaces. he cement slurry seeks the path of least resistance during pumping, which results in more cement slurry remaining in the edge area due to the lower packing density. To maintain a uniform microstructure and achieve a consistent surface finish at the formwork, it is essential to fill these voids with finer particles [37, 45]. A higher packing density represents a more efficient utilization of aggregates, and it holds a pivotal role in minimizing the concrete density [37].

The cement slurry seeks the path of least resistance during pumping, which results in more cement slurry remaining in the edge area due to the lower packing density.

1.3 Pre - wetting of aggregates

Pre-wetting, as elucidated by Assaad and Daou in 2014 [5], is a fundamental technique within the realm of construction. This process involves saturating porous materials before the infiltration phase, and it plays a pivotal role in ensuring the success of the infiltration process.

The primary objective of pre-wetting is to thwart the extraction of water from the cement slurry during infiltration. This precaution serves to maintain the crucial water-to-cement ratio, thereby reducing internal friction and the occurrence of solid particle collisions within the slurry. This optimization, in turn, facilitates the efficient infiltration of the slurry into porous materials. Filtration is a process in which the mortar penetrates a channel [30]. Initially, the mortar successfully infiltrates the channel. A mound of mortar then forms over the channel, forming a filter cake through which only water can penetrate. When the pressure increases, the filter cake partially breaks up, which leads to a renewed infiltration of mortar. However, the cycle repeats itself as the mortar piles up again over the channel, leading to an interruption in flow due to the formation of blockages. This sequence demonstrates the dynamic nature of the filtration process, which involves a constant interplay between mortar penetration, filter cake development, pressure fluctuations and blockage formation. This process is illustrated in the following figure 1.2.

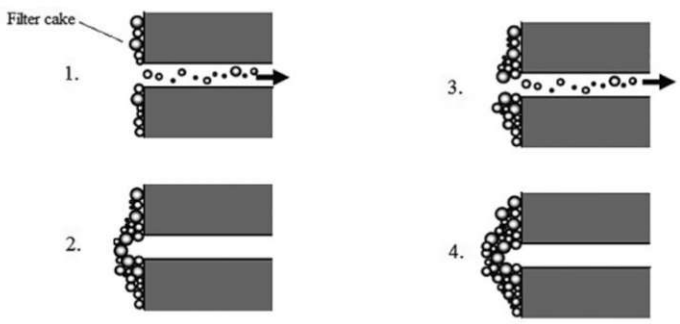

Fig. 1.2: Illustration of filtering process [30].

1.4 Thermal conductivity

The measurement of thermal conductivity holds a critical role in the characterization of construction materials, as it enables the assessment of a material's ability to transfer heat [43]. In the case of structural lightweight concrete, the determination of thermal conductivity is of particular significance. Structural lightweight concrete, in contrast to standard concrete, displays a lower thermal conductivity, primarily owing to the porosity of the aggregate, which is contingent on the type and quantity of aggregate used. It is noteworthy that an increase in bulk density corresponds to an increase in thermal conductivity. These attributes highlight the utilization of lightweight concrete in construction projects, as it not only enhances thermal insulation but also contributes to bolstering the energy efficiency of buildings [32].

In the following table we provide the approximate average thermal conductivity of lightweight concrete according to DIN 4108 [10] and Önorm B4710-2 [32], depending on bulk density.

Wärmeleitfähigkeit Leichtbetons nach DIN 4108		
Rohdichteklasse	Rohdichte (kg/m³)	Wärmeleitfähigkeit (W/(m·K))
D 1,0	800	0,39
D 1,0	900	0,44
D 1,0	1000	0,49
D 1,2	1100	0,55
D 1,2	1200	0,62
D 1,4	1300	0,70
D 1,4	1400	0,79
D 1,6	1500	0,89
D 1,6	1600	1,0
D 1,8	1800	1,15
D 2,0	2000	1,35

Fig. 1.3: Thermal conductivity of lightweight concrete according to DIN 4108 [10].

1.5 Moisture states of grains

In order to ascertain various parameters such as particle density, water absorption, and solid volume fraction, having detailed information about the characteristics of the particles being utilized is crucial. Consequently, Önorm EN 1097-6 [33] describes the moisture conditions applicable to the rock particles or beads employed in these tests. In the case of expanded clay beads, when observed at a microscopic level, it becomes apparent that an aggregate possesses both water-accessible and inaccessible pores. The accessible pores may be either partially or completely saturated with water. To provide a more vivid depiction of this characterization, please refer to Figure 1.4.

The ÖNORM EN 1097-6 [33] defines the four different moisture states as follows:

- Oven dry: The aggregate is completely devoid of moisture, and as a result, each pore remains unoccupied. To attain this state, it is necessary to heat the aggregate to a temperature of 110 ± 5°C until no further change in weight is detected.
- Air dry: Considering factors such as ambient humidity, it's possible for the aggregate to retain some degree of moisture.
- Saturated, surface dry (SSD): All the accessible pores are saturated with water, while the primary surface of the grains remains dry.
- Wet: All the pores that can be accessed by water are completely filled with water, and the primary surface of the grains is wet.

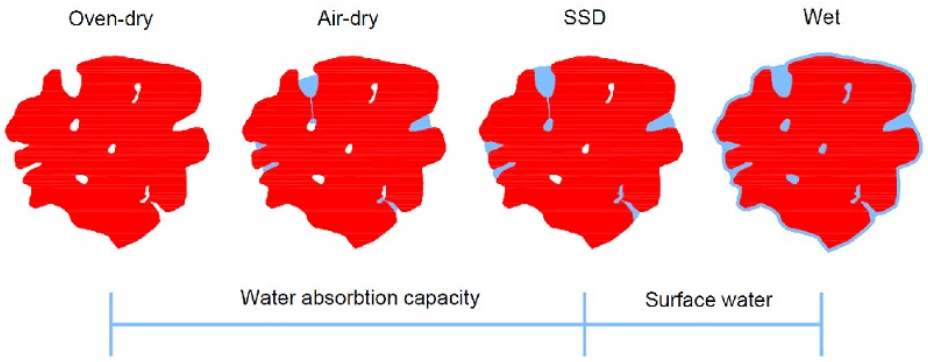

Fig. 1.4: Moisture states of aggregates [36].

1.6 LC^3 properties

As highlighted in the introduction, the environmental factor is becoming increasingly important due to the environmental impact of concrete manufacturing. To achieve favorable outcomes in this pursuit, it is crucial to reevaluate the existing approach to mitigating CO2 emissions in the cement industry [41]. The continuation of this strategy presents challenges due to the restricted availability of conventional cementitious admixtures. Therefore, it becomes imperative to explore new forms of cementitious additives to facilitate this approach. However, the limited availability of cementitious additives in many countries is a barrier to wider application. Currently, more

than 80% [41] of cementitious admixtures used to reduce the clinker content in cement consist of materials such as limestone, fly ash or slag [41]. Calcined clays, especially in combination with limestone, offer significant potential as partial replacements for clinker in cement and concrete. Fig. 1.5 shows the typical recipes of ordinary portland cement (OPC) and LC^3. OPC consists of 95% clinker and 5% gypsum. The energy required for production is high, and the resulting CO_2 emissions are correspondingly substantial. Therefore, efforts are made to reduce the clinker content and replace it with calcined clay and limestone to achieve better CO_2 values. This can save up to 50% clinker. Through the utilization of LC^3, it is possible to reduce CO_2 emissions by up to 40% [22]. This can be attributed to the composition of LC^3 which consists of cement, calcined clay, and limestone. The latter two components are readily accessible and cost-effective, requiring no costly modifications to existing cement facilities. It is also important to highlight the reasons behind the achievable savings, primarily because gypsum and limestone have low global warming potential [8]. During the production of calcined clay, CO_2 is emitted due to the heating to 800°C [22]. Our initial choice was a mixture of limestone, calcined clay and cement (LC^3) [22]. Standard $LC^3$50 consists of 50% clinker, 30% calcined clay, 15% limestone and 5% gypsum. The additional gypsum is already present in the majority of cements at a proportion of approximately 3-7%. The nomenclature LC^3X, where "X" denotes the clinker content in the mixture, and the remaining content consists of a calcined clay to limestone ratio of 2:1 [4].

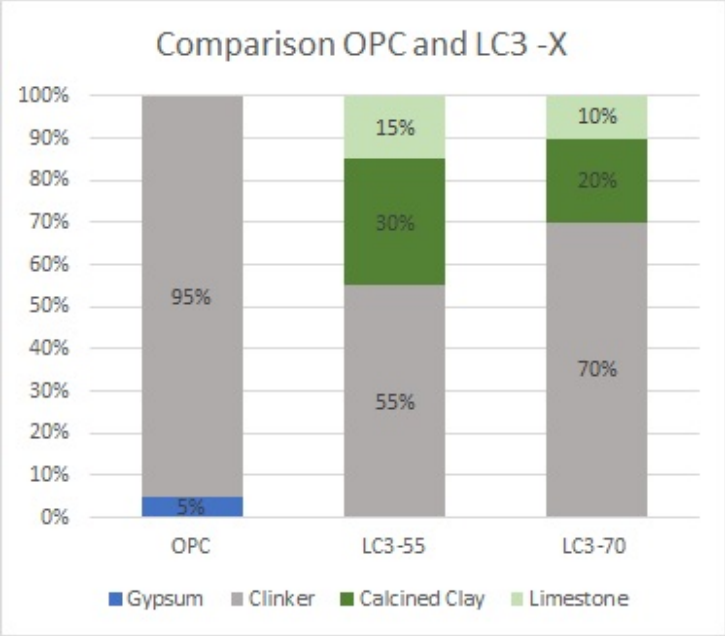

Fig. 1.5: Comparisson OPC and LC3

Chapter 2

Material and Methods

2.1 Materials

In our study, we conducted several tests with different slurries to investigate their infiltration properties. Only the tests in which no blockage occurred, the pipe did not break and the maximum pressure limits of 20 bar were not exceeded are documented here. The first test was perfromed using a mixture of cement and microsilica, while the second test used $LC^3$70. In this section, the used materials are detailed.

2.1.1 Cement

Holcim cement – Der Blaue CEM I 52.5 R was used in all slurries. This cement is categorized as a high-performance cement, as it exhibits an high early strength, reaching around 41 MPa after just 2 days. Moreover, it also attains a remarkable strength after 28 days, consistently meeting the desired minimum of 52.5 MPa [20]. The particle size distribution was analyzed using a Mastersizer 3000, and the results are shown in Figure 2.1. The measurements are from an average of 5 measurements and yielded a D10 value of 3.12 μm, a D50 value of 13.5 μm, and a D90 value of 38.4 μm.

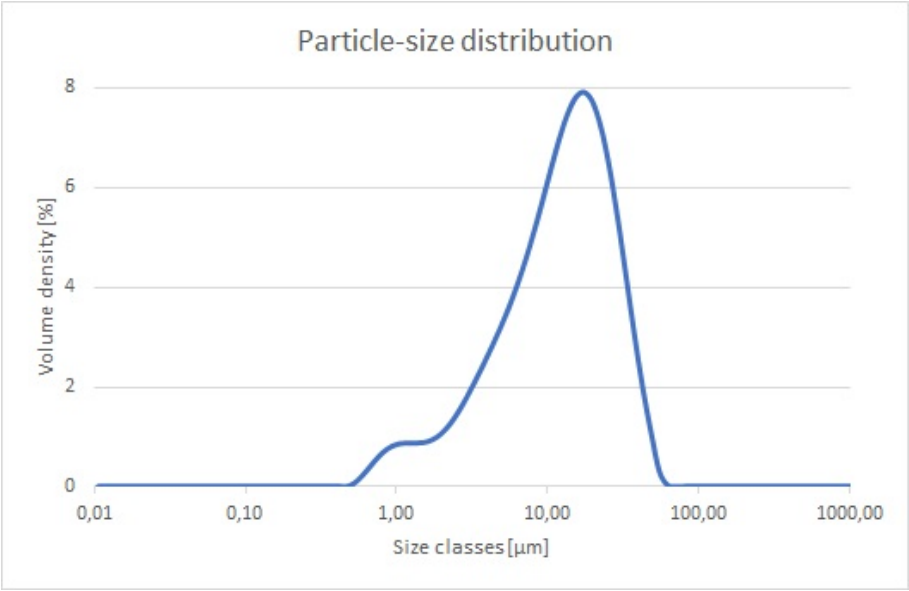

Fig. 2.1: Particle-size distribution of cement Der Blaue.

As can be clearly seen in the figure 2.1, the first hill represents the proportion of gypsum, with a small proportion of fine particles representing the composition, and the subsequent rise is the coarser particles of cement.

2.1.2 Expanded clay beads

Laterlite expanded clay, from laterlite [39] (i.e LECA), is a versatile construction material known for its lightweight (from approx. ρ=320 kg/m³), excellent thermal insulation (λ=0.09 W/mK), and sound-absorption properties. It is fire-resistant (Euroclass A1) and extremely durable [39]. Moreover, it is eco-friendly and widely used in construction, offering high drainage capacity. These materials find applications in a wide range of uses, such as flat and sloping roofs, as a base layer for floor finishes, lightweight insulating backfill, insulation for foundations and earth retaining walls, roof voids, lightweight structural cast concrete, landscaping and roof gardens, blocks and small precast elements, including refractory products, as well as in geotechnical engineering and road construction [24]. The spherical granules come in different size ranges, such as 0/2 mm, 2/3 mm, 3/8 mm, and 8/20 mm [39]. For our experiments we used the sizes 3/8 mm and 8/20 mm (Fig.2.2). You can find the technical characteristics in table 2.1.

Particle size [mm]	0/2	2/3	3/8	8/20
Bulk-density ρ [kg/m³]	680	480	380	350
λ [W/mK]	0,12	0,10	0,09	0,09

Tab. 2.1: Technical characteristics laterlite LECA [39].

(a) Bead size 8/20 mm. **(b)** Bead size 3/8 mm.

Fig. 2.2: Expanded clay beads.

2.1.3 Calcined clay

The clay we used to make LC^3 is a product from Newchem [31]. It is called Metaver N and is produced by calcination of concentrated kaolin and is a slightly reddish, mostly amorphous alumosilicate reacting with cement to precipitates C(A)SH-phases. A particle size distribution, carried out in the figure 2.3, is shown [31]. The Metaver N has a specific density of about ρ = 2.6 g/cm³ and a bulk density between 380 and 520 kg/cm³. Its particle size distribution, shown in fig.2.3, has a D50 of 5.8 μm and a D90 of 14.3 μm.

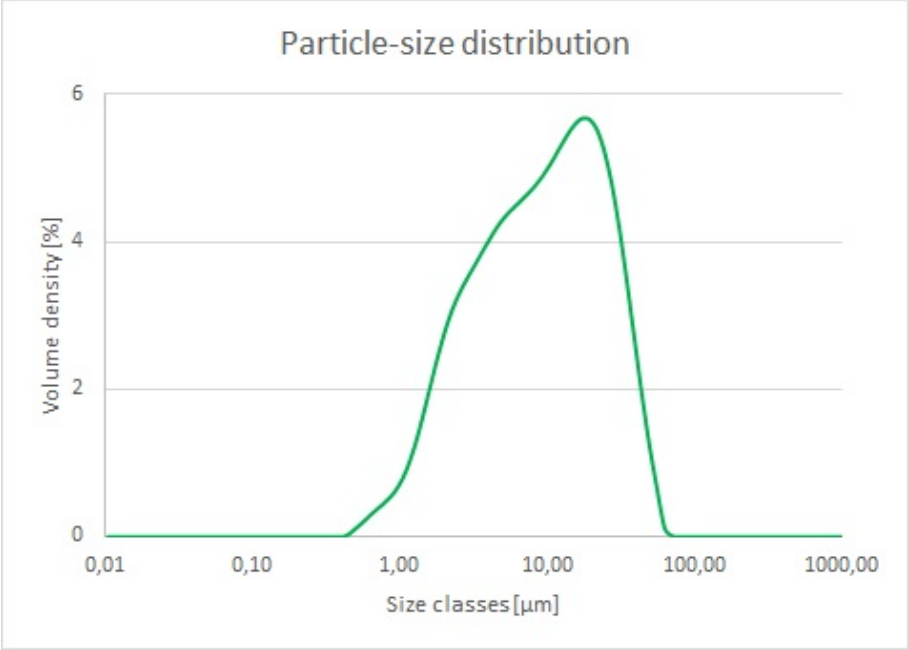

Fig. 2.3: Particle-size distribution of clay Metaver N "slow".

We had a choice of six different types of calcined clay provided by the Newchem [31] company for our study. These six variants mainly differed in their particle size distribution (D10, D50, and D90), color (gray, white, pink, brown, beige), and reactivity, categorized as "slow", "medium", "rapid" and "very reactive".

2.1.4 Limestone

For our experiment, specifically the pump test using an LC^3 mixture, we required limestone powder ($CaCO_3$) was required and we sourced from the company Bernegger [7]. Additionally, we made a particle size distribution (Fig.2.4) analysis for this material. These measurements, based on an average of five readings, provide a D10 of 3.09 μm, a D50 of 15.1 μm and a D90 of 58.9 μm.

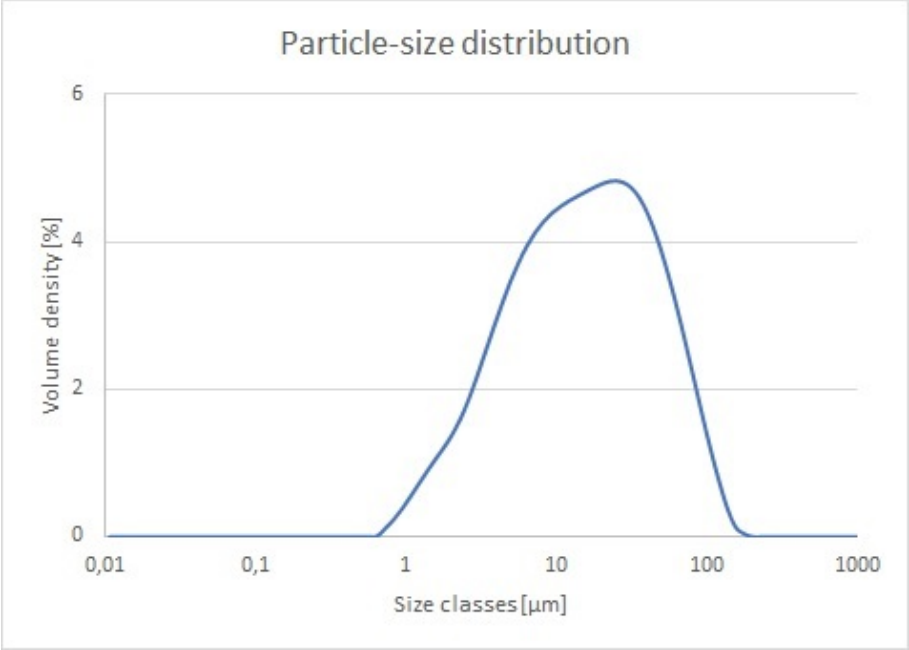

Fig. 2.4: Particle-size distribution of limestone KSM H100.

2.1.5 Superplasticizer

In this research project, the use of superplasticizers was necessary. The PCE-based Master Glenium ACE 430 from Master Builders Solution was used [27]. Superplasticisers are synthetic polymers that have different chain lengths and structural configurations.

One of the main advantages of superplasticisers is their remarkable ability to significantly reduce the amount of water needed for concrete mixing, by up to 30% [42]. This reduction of water used in a mixture does not affect the low yield stress of concrete.

The PCE-based superplasticizer chosen for this study has a density of 1.06 g/cm³. To ensure uniform dispersion, the superplasticizer was consistently dissolved in tap water before its addition to the cement mixture [29].

2.1.6 Retarder

To keep the rheological properties of the cement pastes constant during each infiltration test, we had to delay the process with a retarder. In this case, we used "MasterSure 930", a water-based solution containing polycarboxylic acid salts, with a density of 1.10 g/cm³, manufactured by the Master Builders Solution company [28].

2.1.7 Other used materials in this study

In the initial tests, we used conventional aggregates.
For the subsequent experiments, we also incorporated Elkem D920 microsilica (Fig.2.5) into our mixtures [14]. Microsilica is typically used in ultra high performance concrete (UHPC), as its particle diameters are about 0.15 μm, 100 times finer than those of cement. Due to the fineness of these particles, they act as micro-fillers between the cement particles, increasing the packing density of the entire mixture. The round particles positively impact the rheological properties of the concrete, as they function similar to a lubricant [38].

Fig. 2.5: Elkem's microsilica D920 [14].

2.1.8 Formulation of the pastes

Two different slurries were used for all pumping tests. In each of these tests, the slurries were pumped into three different particle sizes of Leca beads. In the first test, a mixture of only cement and microsilica was used. The amount needed for one test was determined, using a total of 12 kg of cement, 10% of which was microsilica, which amounted to 1.2 kg. The water/cement ratio (w/c ratio) was 0.35, which gave a water volume of 4.20 liters. In addition, 50 g of superplasticizer and 25 g of retarder were added.

In the second test, an $LC^3$70 blend was used. The total amount of mix was 16 kg, divided into 11.20 kg of cement (70% of the total mass), 4.0 kg of calcined clay (25% of the total mass) and 0.8 kg of limestone (5% of the total mass). Again, a w/c ratio of 0.35 was used, with higher amounts of superplasticizer and retarder added. The amount for the former was 78.67 g and for the latter 33.32 g, as shown in table 2.2.

Material	**Test 1 (T1)** Cement & microsilica	**Test 2 (T2)** $LC^3$70
Cement [kg]	12,00	11,20
Water [l]	4,20	5,6
Microsilica [kg]	1,20	-
Calcined clay [kg]	-	4,00
Limestone [kg]	-	0,8
Superplasticicer [g]	50,00	78,67
Retarder [g]	25,00	33,32

Tab. 2.2: Formulation of the used slurrys

2.2 Methods

In this section, the methods and set-ups used for these test experiments are presented to get a better insight and understanding of the results afterwards. In this work all experiments were made at constant temperature and humidity. The laboratory provided consistent temperature of

approximately 23°C ±1.0°C and a humidity of approximately 40% ±10%. After the experiments, the samples were covered with foils to prevent premature drying on the surface of the material. All materials used were stored and hardened under these conditions.

2.2.1 Mixing protocol

Uniformity in the trials was ensured by the preparation of a mixing protocol, which was followed each time a experiment was conducted. It is known that the mixing intensity, measured in rotations per minute (RPM), and the mixing duration influence the properties of the fresh concrete mix [2]. Higher RPM and longer mixing decrease yield stress and viscosity by increasing superplasticizer adsorption on cement particles. In all experiments where a pumping test was conducted, a hand mixer (Fig.2.6) of the brand Einhell, model TE-MX 1600-2 CE Twin, was used. The procedure we followed for our mixes is defined as follow:

- Weighing of materials: The various materials such as cement, water, clay, limestone powder, superplasticiser and retarder were weighed.
- Dry mixing: In a first step, the base materials were mixed dry, without superplasticiser and the retarder.
- Water and superplasticiser: Half of the superplasticiser was added to the water container and then slowly added to the dry mix.
- Mixing - initial phase (180 seconds, slow): The mixture was mixed slowly for 180 seconds in the initial phase.
- Mixing - second phase (180 seconds, faster): The mixing speed was then increased for another 180 seconds.
- Waiting time (120 seconds): There was a short pause of 120 seconds.
- Mixing - final phase (60 seconds) with addition of residual superplasticiser and retarder: In this phase, the residual superplasticiser and retarder were added to the mixture. The mixture was then mixed for further 60 seconds.
- Spread and Funnel Test: After the mixing process, the consistency and workability of the mixture were evaluated through the performance of a spread test and a funnel test.

The reason for a two-stage mixing process [3] is to improve the concrete properties. The improving effect of the gradual and delayed addition is related to the interaction between cement and superplasticizer during the initial hydration phase of the cement, which is influenced by the cement activity and the adsorption behaviour of the superplasticizer [26].

Fig. 2.6: Using the handmixer.

2.2.2 Set up

Initial injection set up The original setup was done by a master's student named Lukas Pointner [34], whose work is continued here. This setup included a wooden frame to fix the pipe using pipe clamps and a funnel with a ball valve to pump the slurry into the pipe. However, this original set-up proved unsuccessful, resulting in the need to redesign or find a solution. The first challenge was to create a seamless transition from the tube to the funnel. To accomplish this, three ultra-high performance concrete (UHPC) plates were used. The shape of the funnel was taken into account when making these panels to ensure a perfect fit (see fig.2.7). As the initial fixing using pipe clamps was insufficient, two additional holes were drilled in the slab to accommodate threaded rods. These rods were to be used to hold the pipe in place and apply pressure. A frame was then welded to fit the slab, and a steel mould tube was made and attached to the top using the threaded rods to press the tube into the funnel (see fig.2.8). The two other plates were supported using concrete prisms.

When switching to a cement-based slurry, persistent leaks between the hopper and the pipe required alternative solutions. The initial silicone seal proved inadequate, especially at higher

pressures, so we used a hot glue gun for a more secure seal. The subsequent integration of a pressure sensor involved welding steel tabs onto a nut corresponding to the sensor diameter and attaching them to the pipe (see fig.2.9b) together with the sensor using tensioning straps. To prevent Leca particles, especially smaller diameters, from entering the funnel or the hose, a wide-mesh reinforcement mesh was attached to the base of the pipe. This mesh, taken from the facade plaster, was stretched over the lower end and then secured with a cut-off sleeve and a sealing ring (Fig.2.10a). To prevent leaks at the transition from the hose to the funnel, the initial experiments with hose clamps were replaced by a wooden plate with holes for the escape of air and slurry, secured at the top by a steel beam. The entire setup, its modifications and improvements are shown schematically in the figures 2.7 and 2.12, while the comprehensive test results are listed in the appendix.

The process that led to the final setup can be summarized as follows:

Our initial approach was to attach the hose to the hopper using various hose attachments. However, we had difficulty making a secure connection. We then moved to the next step, which was to use a hose-to-hose transition piece so that we would no longer be dependent on the hopper. In this configuration, one end of the tube was tucked into the transition piece, while the other end was covered with a rain barrel and hose connector that has a hole for attaching a fitting. This connector provides a better surface for the hose, preventing it from slipping. We used two hose attachments each. Although this was an improvement, we found that placing the set up in the fit of the funnel did not work as the footprint was too small and the lid kept breaking due to the pressures at the bottom. Therefore, we came up with the idea of turning the UHPC plate around to get a larger bearing surface for the lid (see fig. 2.10b). This worked better, but the lid continued to break, so a formwork panel was cut to the diameter of the connector to provide even more bearing surface. The next step was to replace the wooden plate on top with a lid. This new lid was not only watertight, but also allowed the controlled drainage of the sludge coming in from above.

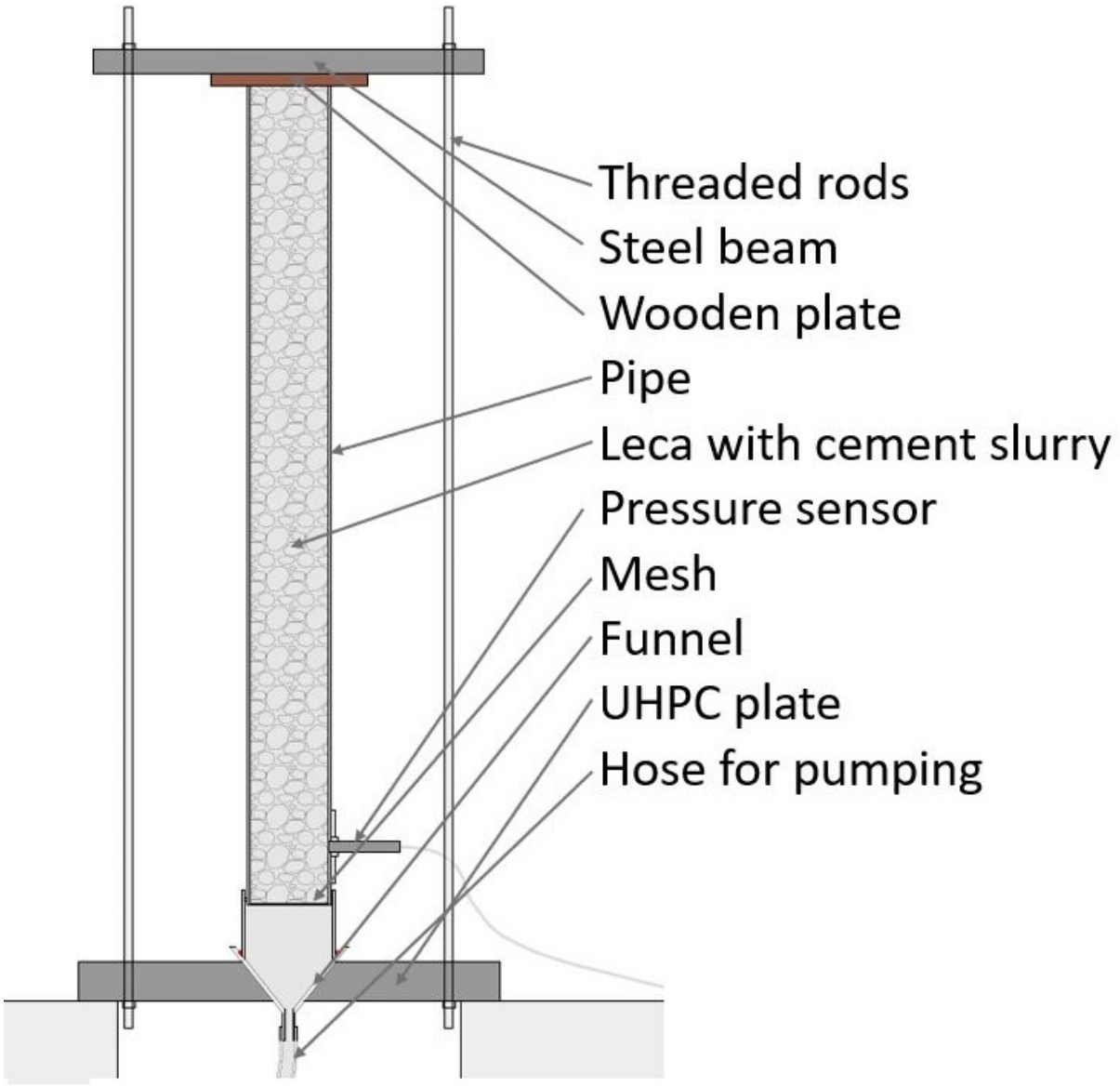

Fig. 2.7: Initial injection set up including labeling.

Fig. 2.8: Initial set up

(a) Funnel fixing.

(b) Sensor fixing.

Fig. 2.9: Initial set up attempts.

(a) First mesh attempt.

(b) Set up without wooden plate.

Fig. 2.10: Initial injection set up preparation.

Injection set up Our home custom injection set up is shown in fig. 2.12 and fig. 2.13. It consists of a plate of UHPC (ultra-high strength concrete), to which four threaded rods are attached. To fix the pipe was welded together a cross of metal, which can be fixed with nuts. This plate including rods can be placed either on a specially welded stand or on concrete prisms.

The structure used for the experiments consists of a tube to which a lid is attached. This lid serves on the one hand to retain the leca in the pipe and on the other hand to collect the cement paste in a controlled manner and to collect it in a container. The pipe used for the experiments was either an orange polyvinyl chloride (PVC) pipe with a diameter of 11 cm or a transparent plexiglass pipe completely filled with leca. In the lower part of the tube, a holder for a net was attached with the help of screws and internal seals. These net serves to hold the contents (Fig.2.11a) (expanded clay beads) in a certain position. Directly below the net is a hole and a holder for a pressure sensor. This sensor is fully welded with a flush diaphragm from the company Baumer. To ensure a functional transition that can withstand the existing pressures, a pipe transition was attached to the pipe where on one side the pipe is inserted and on the other side a cover and a seal are used for closing. A hose connection adapter (see fig. 2.11b was integrated into the cover, which establishes the connection by means of a hose to the eccentric screw pump.

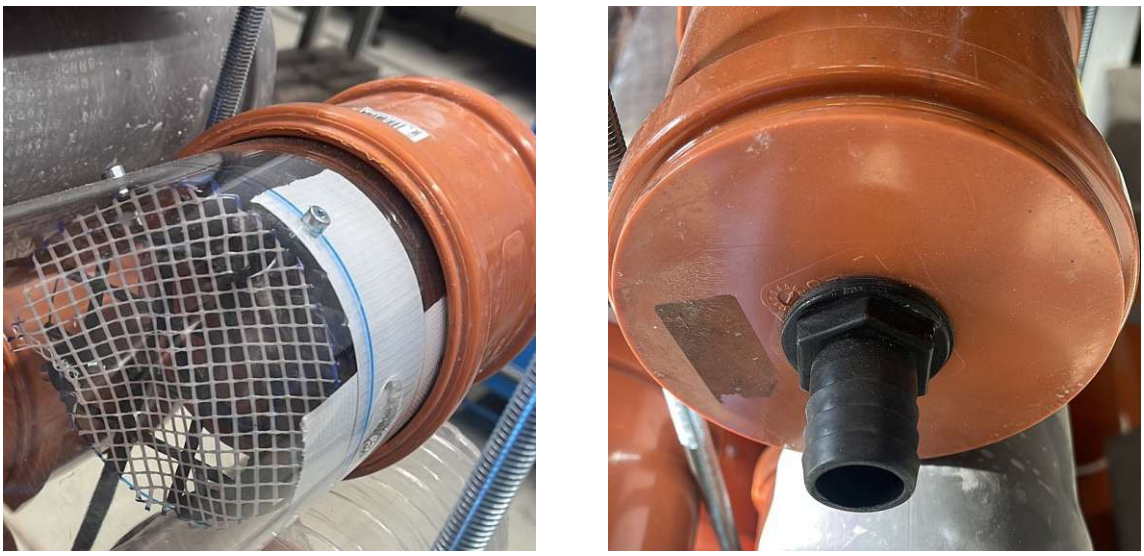

(a) Mesh to fix the beads in the pipe **(b)** Hose connection adapter

Fig. 2.11: Injection set up preparation.

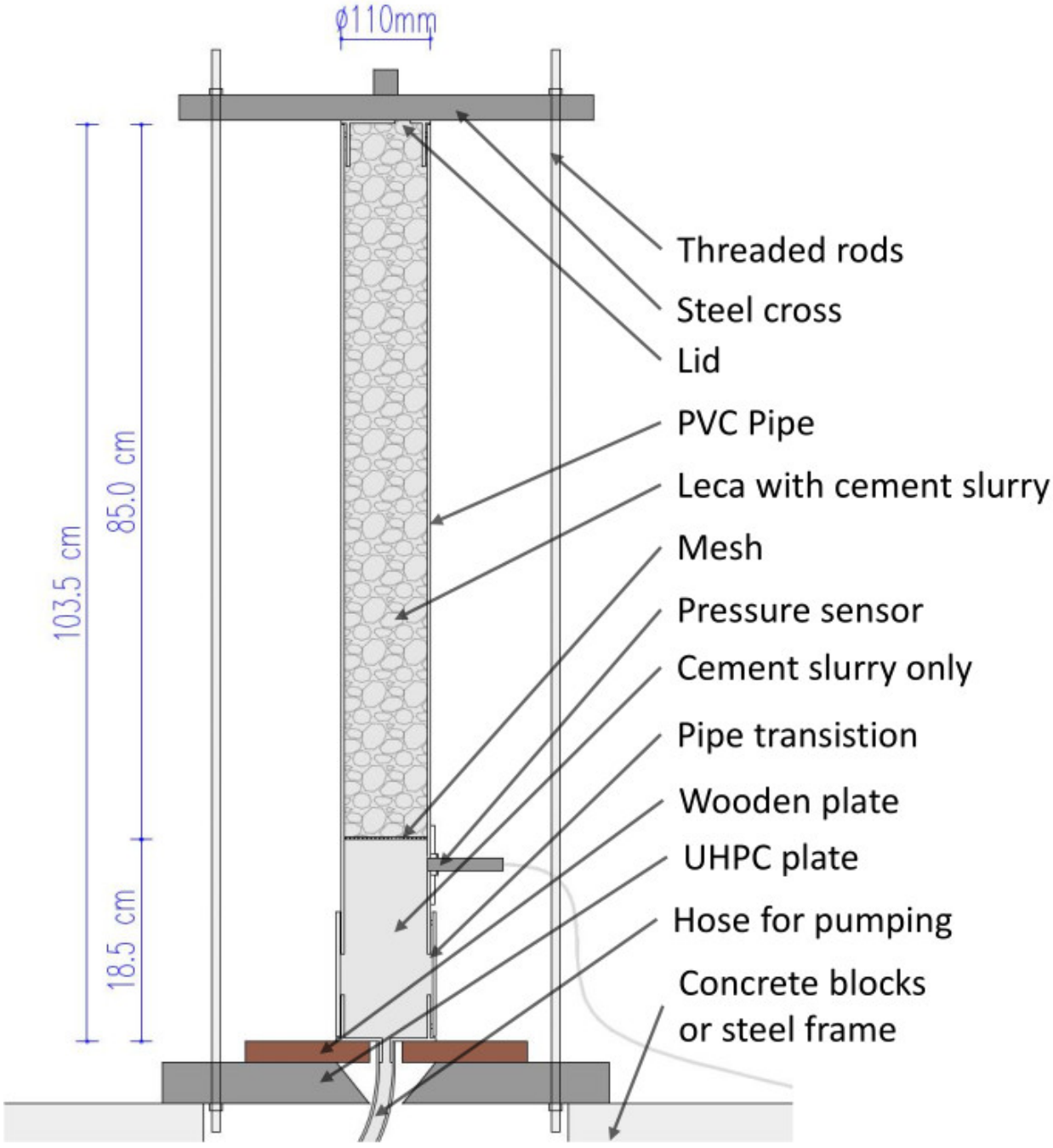

Fig. 2.12: Injection setup including labeling.

Fig. 2.13: Picture of injection set up.

2.2.3 Infiltration procedure

Before each test, the same sequence of steps was always performed to configure the setup. To ensure a clear overview, the steps were listed below:

1. Cut the pipe.
2. Drill a hole in the lid for the hose-to-pipe transition piece.
3. Drill a hole in the pipe for the pressure sensor.
4. Tape the hole with tape.
5. Drill a hole in the pipe for net attachment.
6. Fix the screws with sealing rings.
7. Secure the net.
8. Attache the hose-to-pipe transition piece to the lid.
9. Assemble the lid and transition piece.
10. Connect the transition piece to the pipe.
11. Fix the hose piece.
12. Weigh the pipe.
13. Fill the pipe with Leca and weigh it.
14. Prepare the frame with UHPC plates, rods, and the wooden plate.
15. Secure the filled pipe on the frame.
16. Attache the lid on top and fix the hose.
17. Secure the whole setup.
18. Fix the pressure sensor.
19. Prepare the laptop to measure the pressure.
20. Assemble the pump.
21. Test the pump with water.
22. Prepare the hose.
23. Prepare and weigh the materials (cement, clay, water, limestone, retarder, superplasticizer).
24. Prepare the mixer.
25. Mix according to the mixing protocol as demonstrated in section 2.2.1.
26. Carry out a spread and funnel test.
27. Pour the slurry into the pump container.
28. Turn the pump on and let the slurry run for about 20 seconds.
29. Do a sensor function test.
30. Turn the pump off and connect the hose to the set-up.
31. Start the pumping process.

After completion of each test, the hose was first disconnected at the bottom to prevent material from leaking out of the tube. Disassembly of the hose from the setup then took place, followed by cleaning of the pump. The pressure sensor was removed and safely stowed, and all tools used, such as the trowel and pan, were thoroughly cleaned. Finally, the lid of the setup was removed, and a film was placed over the pipe to prevent premature drying of the material surface.

2.2.4 Spreads test

The spread test is used to determine the yield stress of a cement slurry, using a standard Hägermann-cone (Fig.2.14a and 2.14b). The cement slurry is poured into a conical container without any shaking. The cone is placed on a slightly moistened level surface that is free from any roughness that could affect the flow of the suspension. Once the cone is fully filled, it is lifted upwards, and the suspension spreads out in a circular pattern (Fig.2.15).

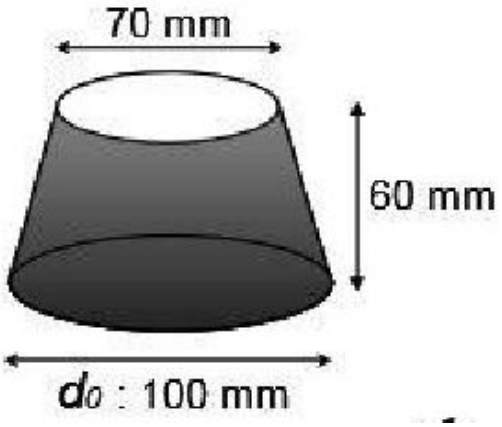

(a) Hägermann-cone [12].

(b) Cone for spread.

Fig. 2.14: Visualization of the cone.

The spread measurement (Fig.2.15) is determined by taking two perpendicular measurements of the spread suspension and averaging them. With the spread measurement the yield stress can be calculated with the following equation (2.1)

$$\tau_0 = \frac{225\rho g V^2}{128\pi^2 R^2} \tag{2.1}$$

Fig. 2.15: Spread measurement.

2.2.5 Funnel test

After the spread test, a funnel test was performed to get a feel for the viscosity of the cement slurry. For this purpose, we used a funnel with a capacity of 1.10 liters, the dimensions can be seen in fig.2.16. For the test, the funnel was completely filled, and the top was then smoothed. Afterwards the time was measured from the moment the shutter was opened at the bottom of the funnel to the time when there was visibility through the entire funnel. It indicates a quantitative between time and viscosity of a slurry.

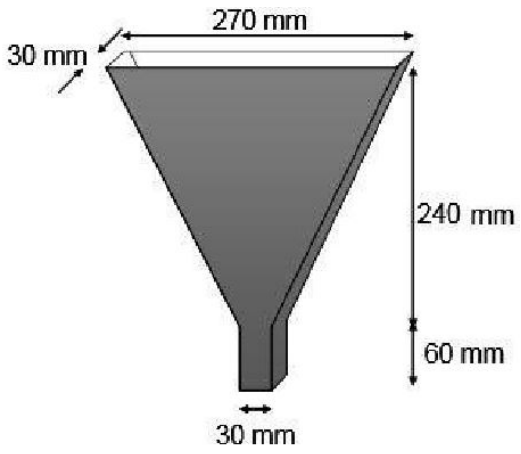

(a) Funnel dimension [12].

(b) Funnel in the lab

Fig. 2.16: Visualization of funnel test.

2.2.6 Leca beads characterization

To gain information about the expanded clay beads we used in our research, we did various tests. These tests helped us better understand the properties of these beads, which were important for our studies.

2.2.6.1 Drying test

The moisture content of the Leca beads is specified on the packaging. In order to perform accurate calculations with the Leca beads, we are interested in their moisture content on the one hand, and on the other hand we would like to understand how the Leca beads behave during infiltration. To obtain this information, we performed an evaluation to determine the exact moisture content of the expanded clay beads directly from their packaging. For this purpose, we performed a drying test with two different sizes of beads, 3/8 mm and 8/20 mm, in aluminum containers. First we weighed the empty aluminum container, then the container with the beads, and we repeated this process for both sizes. Then we placed both containers in an oven and dried them at 100 °C for 120 hours.

2.2.6.2 Water absorption test

As water is present in our mixtures during infiltration, we are interested in how effectively the porous beads can extract water from the cement slurry during the infiltration process. To determine the water absorption of the expanded clay beads, we proceeded as follows: First, the expanded clay beads were carefully dried in an oven to ensure that no residual moisture was present. Then we placed them in a suitable container and kept them under water with a net. This step was crucial because the clay beads would otherwise float on the surface due to their lower density compared to water and thus would not be able to absorb water.

In our investigation, we measured the weight of the clay beads at various time: after 60 seconds, 120 seconds, 60 minutes, 120 minutes, and after 12 and 24 hours. As container we used a conventional pyknometer, but we modified it using a 3D printer by creating a mesh (Fig.2.17). The beads were removed from the container and the excess water on the surface was wiped off with a damp cloth. It is important to note that the values measured by this method may be subject to uncertainties. This is because it is difficult to determine the exact amount of retained water or trapped air bubbles in the 3D printed mesh and the silicone used for fixation. Throughout the experiment, efforts were made to remove air bubbles from the clay beads by using an IKA Vortex 3 to "agitate" the air pores in the clay beads. This was done to ensure that water absorption was measured as accurately as possible.

Fig. 2.17: Pyknometer with mesh.

2.2.7 Particle density

To gather more information about the materials used, we attempted to determine the particle density after conducting the water absorption test. The particle density refers to the density of a bead, whereby closed cavities are not taken into account. However, the volume of open pores, which are accessible for the penetration of cement, is not taken into account in this calculation. This information is essential, as only the bulk density is specified during production, whereas the particle density is required to calculate the packing density. The datasheets for the beads provide only a rough estimate of density, and they specify bulk density rather than the particle density of individual beads. Determining the particle density is a complex task, as some beads are partially broken in the middle, others allow water to penetrate their interior, and still others have closed internal pores. Therefore, we attempted to gain insights into the density using three different tests.

Determination of particle density according to ÖNORM EN 1097-6 For this test we used ÖNORM EN 1097-6:2022 [33]. We used the test described in chapter 8 in ÖNORM EN 1097-6:2022 for the particle sizes 8/20 mm, 3/8 mm and also for the 2/3 mm. Here is a simple summary of the test procedure according to ÖNORM:

- Soak the sample in water at 22 ± 3 °C for 24 ± 0.5 hours, removing air bubbles.
- Weigh the container with the wet sample (M2) and record the water temperature.
- Drain most of the water, refill, and weigh again (M3). Note the water temperature. The temperature difference between M2 and M3 should be within 2 °C.
- Optionally, pre-calibrate volume of the container.
- Spread the wet sample in a tray, gently dry with warm air, and cool to room temperature while stirring.

- Weigh the surface-dry sample (M1).
- Dry it in an oven at 110 ± 5 °C until its weight stabilizes. Cool and weigh again (M4)

The determination of the three different particle densities ρ_{a}, ρ_{rd} and ρ_{ssd} was calculated using the following formula [33]:

$$\text{apparent particle density} \qquad \rho_a = \rho_w \frac{M_4}{M_4 - (M_2 - M_3)} \tag{2.2}$$

$$\text{oven-dried particle density} \qquad \rho_{rd} = \rho_w \frac{M_4}{M_1 - (M_2 - M_3)} \tag{2.3}$$

$$\text{saturated and surface-dried particle density} \qquad \rho_{ssd} = \rho_w \frac{M_1}{M_1 - (M_2 - M_3)} \tag{2.4}$$

Determination of particle density according to Archimedes principle To have another comparison test, we used the idea of Archimedes principle[1], and performed a simple experiment. This principle states that the buoyant force acting on an object in a liquid is equal to the weight of the liquid displaced by the object.

For these experiments, we used as container also the pyknometer with a marked line (Fig.2.18) on it. We also used the the 3D printed net to hold the beads underwater. In this experiment, we did not account for the net, which introduced a certain level of uncertainty.

Three tests were conducted as follows:

1) In the first test (PDT1), the beads were taken directly from the container without prior drying. We attempted to remove air bubbles and shook the container by hand.

2) In the second test (PDT2), the beads were also taken directly from the bag without prior drying. This time, we used the Vortex 3 (see Figure 2.18) to remove air bubbles.

3) In the third test (PDT3), the beads were dried for approximately 24 hours until no further weight change was observed. We then repeated the experiment from T2.

The particle density is calculated using the following formula:

$$PD = \frac{M_{\mathrm{L}}}{M_{\mathrm{WDL}}} \tag{2.5}$$

$$M_{\mathrm{WDL}} = M_{\mathrm{WC}} - M_{\mathrm{WL}} \tag{2.6}$$

with:

PD	Particle density $[kg/m^3]$
$\mathrm{M_{WC}}$	Container filled only with water to mark $[g]$
$\mathrm{M_{WL}}$	Mass water when Leca in container $[g]$
$\mathrm{M_{WDL}}$	Mass water displaced by Leca $[g]$
$\mathrm{M_L}$	Mass of Leca in container $[g]$

Fig. 2.18: use of Vortex 3.

2.2.8 Packing bead density

As already described in section 1.2, achieving a high packing density of the aggregate is important in order to obtain minimal concrete density. The packing density was measured in three different ways: first with the prepared samples and back calculation with cement, second by filling the tube with water while the beads were in the tube, and third with the imaging software Fiji ImageJ software [40].,

Packing of beads in pipe with water To determine the packing density using water, we initially filled a tube completely with water to measure the maximum amount it could hold. Then, we filled the same amount of water that fit into the tube into a bucket, which was measured using a scale. Afterward, the tube was dried again, and the height of the net was measured. Different bead sizes were then placed in the tube and positioned. Next, water was added from the top, and during this process, gentle tapping on the tube with the hand was done to remove air bubbles. The tube containing the granules and water was left to stand for a while to allow water to penetrate the voids. After multiple tapping sessions and approximately one hour of waiting, water was again added up to the top of the tube, and the remaining amount of water was weighed. This provided us with the measured values. An estimate of the packing can be made by using the following equation:

$$P = 1 - \frac{V_{\mathrm{w}}}{V_{\mathrm{w}}} \tag{2.7}$$

with:

P	Packing [-]
V_w	Volume of water inside the pipe $[m^3]$
V_w	Volume insde of the empty pipe $[m^3]$

Packing in hardened concrete After successfully pumping out the pipes with the three different bead sizes of Leca, samples were taken from both experiments: the first experiment involving cement and microsilica, and the second experiment with an $LC^3$70 mixture. For this purpose, the

tube was divided into five equal sections (cut every 15 cm) (see fig.2.19a and fig. 2.19b). Before the tests, the weight of the beads was measured, and the position of the net was determined, allowing for a back calculation using the weight and density of the cement. Consequently, each sample was measured in terms of diameter and height and additionally weighed. With this information, it was possible to determine the packing density. All sample measurements were taken using calipers and the scale measures accurately to two decimal places and up to 2500g.

The following formulas were used for the calculation:

$$V = \frac{d^2 * \pi}{4} * h_{\text{sample}} \tag{2.8}$$

with:

P	Packing [-]
V	Volume of the sample $[dm^3]$
h_{sample}	Height of the sample $[mm]$

$$\rho = \frac{m_{\text{sample}}}{V} \tag{2.9}$$

with:

ρ	Density of a sample $[kg/m^3]$
m_{sample}	Mass of the sample $[g]$

$$m = \frac{m_{\text{sample}}}{h_{\text{sample}}} \tag{2.10}$$

with:

m	Mass per centimeter $[g/cm]$

$$m_{\text{L}} = \frac{m_{\text{Lc}}}{h_{\text{sample}}} \tag{2.11}$$

with:

m_{L}	Mass fraction of Leca $[g/cm]$
m_{Lc}	Mass of Leca in the container $[g]$

$$m_{\text{c}} = m - m_{\text{L}} \tag{2.12}$$

with:

m_{c}	Mass fraction of cement $[g/cm]$

$$tm_{\mathrm{c}} = m_{\mathrm{c}} * h_{\mathrm{sample}} \tag{2.13}$$

with:

$\mathrm{tm_c}$	Total mass fraction of cement $[g]$

$$tm_{\mathrm{L}} = m_{\mathrm{L}} * h_{\mathrm{sample}} \tag{2.14}$$

with:

$\mathrm{tm_c}$	Total mass fraction of Leca $[g]$

$$V_{\mathrm{c}} = \frac{tm_{\mathrm{c}}}{\rho_{\mathrm{slurry}}} \tag{2.15}$$

with:

$\mathrm{V_c}$	Volume share cement $[dm^3]$
ρ_{slurry}	Density of the slurry $[kg/m^3]$

$$\epsilon = \frac{V_{\mathrm{c}}}{V} \tag{2.16}$$

with:

ϵ	Void content [-]

$$PD = 1 - \epsilon \tag{2.17}$$

with:

PD	Packing density [-]

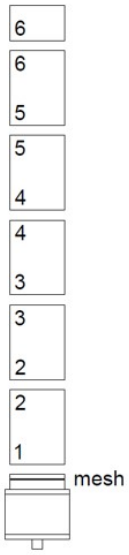

(a) Sections of the pipe.

(b) Cutting the sample

Fig. 2.19: Visualization of sections of the used pipe and samples.

Packing with image analyse As mentioned in section 2.2.8, the analysis of packing density was also conducted using an image treatment analysis program called Fiji, ImageJ [40]. In this process, the cut samples were photographed on each side and subsequently processed and analyzed using the program. For each tube and bead size, a total of 10 photos were analyzed. By setting specific color threshold values, beads could be distinguished from cement. The ratio of the area occupied by the beads to the total area in the tube is defined as packing density.

As seen in the photos (Fig. 2.20), an attempt was made to create a clear distinction between cement and beads using color thresholds (Fig. 2.21). Subsequently, the analysis program was used to determine the area, as shown in the image (Fig. 2.22), with individual colored areas. However, as evident, the program couldn't precisely define the exact boundaries of the beads, resulting in some degree of inaccuracy. To improve the accuracy of the analysis, manual adjustments were attempted to trace the beads by hand. One aspect that is not accounted for is the filling of voids within the beads, as the quality of the smallest particles is not easily discernible to the naked eye. Consequently, there is a cumulative effect of errors that could slightly distort the results, despite the percentage values provided.

Fig. 2.20: Photo of a sample.

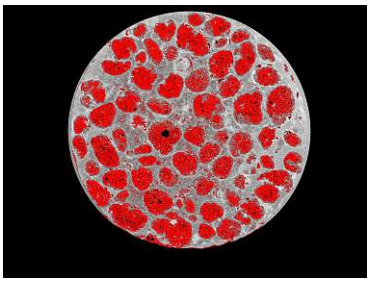

Fig. 2.21: Threshold of a sample.

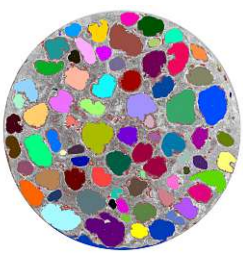

Fig. 2.22: Analyze with program.

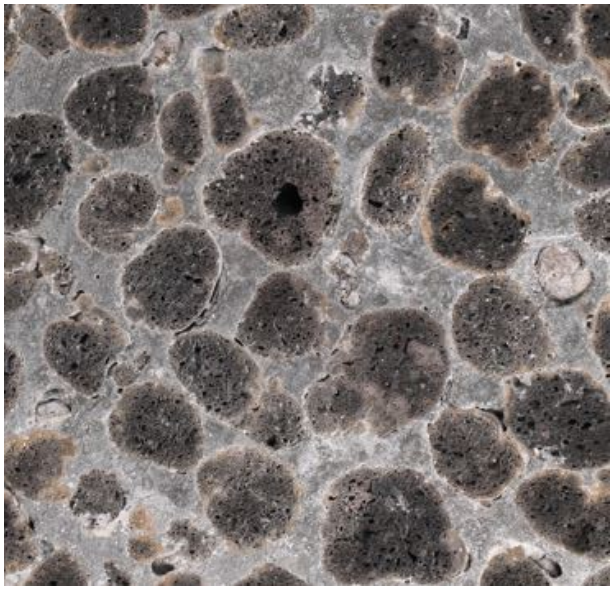

Fig. 2.23: Photo of a magnified sample.

2.2.9 Tests of the samples during and after injection

2.2.9.1 Pressure measurements

In all test experiments, we closely monitored both the pipe pressure (with a pressure sensor, see fig.3.8 and the pump values for safety, as the pump has a maximum pressure capacity of 20 bar. For each experiment, we used a laptop to monitor the pressure sensor and display the values in the form of a diagram. An intermediate piece was placed between the pump and the hose to ensure that the maximum pressure values of the hose and pump were monitored and that the experiment could be stopped if necessary.

2.2.9.2 Compressive strength

Compressive strength testing of the specimens was performed by cutting them into 15 cm long sections and then grinding them. To perform the compressive strength tests, we used Toni Technik's [19] testing machine. Here, the specimens were placed centered between the two plates of the machine, which then applied pressure to the specimen until failure occurred seen in figure 2.19a. The results obtained were carefully documented and can be evaluated in the form of diagrams and tables. In order to obtain an overview of the compressive strengths of lightweight concrete, table 2.25 provides an insight into the lightweight concrete classes according to DIN EN 1992 [16].

Fig. 2.24: Compressive strength test.

Druckfestigkeitsklassen für Leichtbeton nach DIN EN 1992		
Festigkeitsklasse	charakteristische Zylinderdruckfestigkeit (N/mm²)	Mittelwert der Zylinderdruckfestigkeit (N/mm²)
LC12/13	12	17
LC16/18	16	22
LC20/22	20	28
LC25/28	25	33
LC30/33	30	38
LC35/38	35	43
LC40/44	40	48
LC45/50	45	53
LC50/55	50	58
LC55/60	55	63
LC60/66	60	68
LC70/77	70	78
LC80/88	80	88

Fig. 2.25: Compressive strength classes for lightweight concrete according to DIN EN 1992 [16].

2.2.9.3 Thermal conductivity

In figure 2.26, the thermal conductivity test is shown. This experiment was conducted using a Hot Disk M1 with a diameter of 19,8 mm from the company Hot Disk. The flat sensor, as shown in fig.2.26b, serves as both a heat source and a temperature sensor. In standard measurements, it is placed between two identical material samples (Fig.2.26a). Consequently, the disk is heated, and the program calculates the thermal conductivity based on the cooling time of the disk. All tests were carried out after drying in the air.

(a) Testing between two samples **(b)** Hot disk

Fig. 2.26: Thermal conductivity test

Chapter 3

Results and discussion

In this chapter, we present all the results and the corresponding explanations. We start with the characterization of the Leca beads and then document the results of the two different infiltration tests, test 1 (T1) with cement and microsilica and test 2 (T2) with $LC^3$70.

3.1 Leca beads characterization

3.1.1 Drying test

The initial weight measurements (Fig.3.1), up to complete drying, revealed that for the 3/8 mm bead size beads, only 0.37 g of water was extracted from an initial weight of 210.58 g. This corresponds to a percentage reduction of 0.17% of the weight. Similar for the 8/20 mm bead size beads, the difference was nearly identical, with 0.31 g of water and a reduction of 0.15%. These results confirm that the manufacturer's datasheet specification of ±1% humidity is accurate.

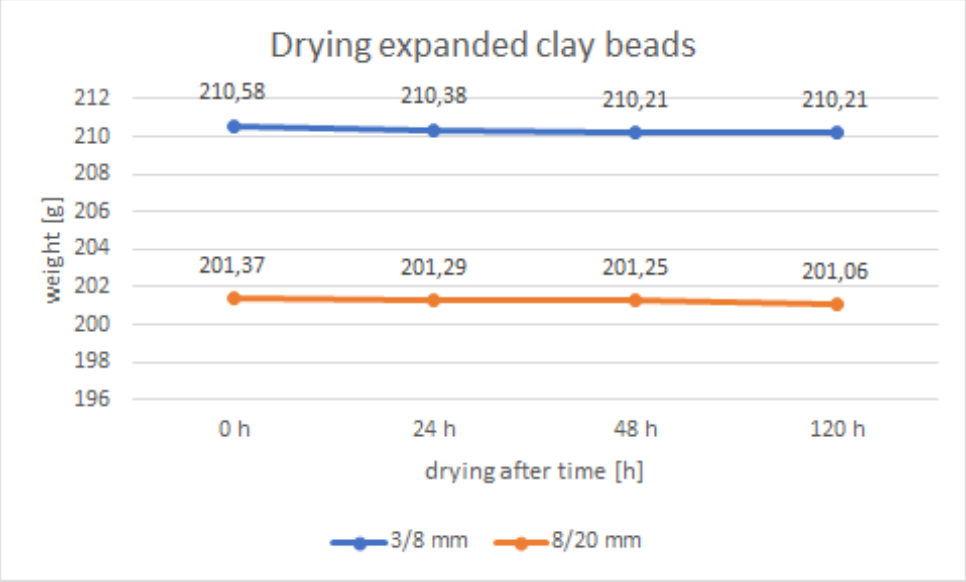

Fig. 3.1: Drying test of expanded clay beads

3.1.2 Water absorption test

The results seen in fig.3.2 clearly show that most of the water absorption occurs early in the process, particularly in the first 60 seconds, and is 6.8% ± 1.5% of their mass for diameters 3/8 mm and 6.5% ± 1.5% of their mass for bead size 8/20 mm. The water absorption is very similar for both sizes, with the most significant differences observed after 12 hours and 24 hours.

After 24 hours, the final absorption for 3/8 mm beads is approximately 13.5% ± 1.5% of the mass, while for 8/20 mm beads, it's about 11.3% ± 1.5% of the mass (Fig.3.2). One possible explanation is that, in both cases, there were significantly more air bubbles in the container after 12 and 24 hours, which could only be removed after using the vibrator. It is possible that these air bubbles had more difficulty traveling through the narrower path within the smaller beads compared to the larger beads. The results of this test show us that the Leca beads are able to absorb a significant amount of water in the first 120 seconds. This could lead them to extract a significant amount of water from the slurry composition, thus changing the properties of the slurry. This highlights the importance of pre-wetting to prevent or at least reduce the extraction of water from the slurry composition.

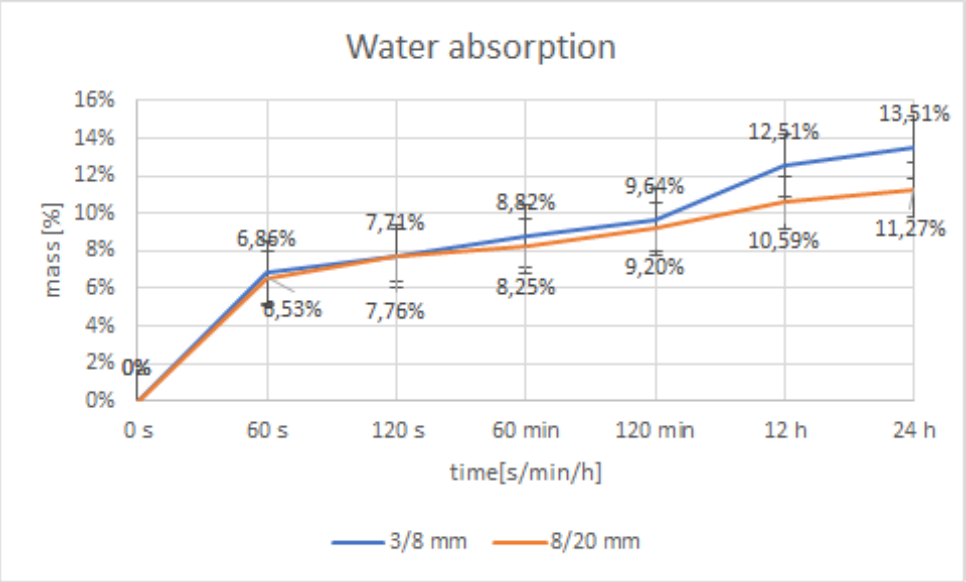

Fig. 3.2: Water absorption test on Leca beads

3.2 Particle density

3.2.1 Determination of particle density according to ÖNORM EN 1097-6

After performing the test in accordance with the instructions provided in 2.2.7, the results for the determination of particle density are presented in the following table 3.1.

	LECA		
	2/3 mm $[kg/m^3]$	3/8 mm $[kg/m^3]$	8/20 mm $[kg/m^3]$
ρ_a	435,29	664,85	601,21
ρ_{rd}	410,74	626,20	577,29
ρ_{ssd}	467,13	684,33	617,07

Tab. 3.1: Particle density according to ÖNORM EN 1097-6:2022 [20].

ρ_a apparent particle density $[kg/m^3]$

ρ_{rd} oven-dried particle density $[kg/m^3]$
ρ_{ssd} saturated and surface-dried particle density $[kg/m^3]$

The results show that for all three bead, ρ_{ssd} is higher than ρ_a which is hihger than ρ_{rd}. This is due to the fact that after drying, there is no residual moisture left in the beads, making them lighter. In contrast, for the other two densities, the pores are still affected by residual moisture, as opposed to being completely saturated. An example of this is the particle size of 8/20 mm, where a mass volume change of 4.14% was found between oven-dried particle density and apparent, and a change of 2.63% was found between apparent and saturated and surface-dried.

3.2.2 Determination of particle density according to Archimedes principle

This calculation is based on the procedure described in paragraph 2.2.7. In the first test (PDT1), beads were used without drying and air bubbles removed by hand shaking the water/bead filled container. The second test (PDT2), beads were also used without drying, but air bubbles were removed using the Vortex 3. And the third test (PDT3) involved dried beads with a repeat of the second test (PDT2). The results of the three different tests with application of Archimedes' principle clearly show that the particle density increases from PDT1 to PDT3 for both particle sizes. This is not only due to the fact that at PDT3 the beads were completely dried, but also due to the application of different methods to remove air bubbles. It is clear that simple hand shaking is nowhere near as effective as using vibration. The difference from PDT1 to PDT2 shows that, although small, the use of the vortex helped to remove air bubbles better and thus gave more realistic results. The test PDT3 achieved the highest density because, during the test, the beads were completely dry, meaning no water was present in the pores before the test initiation. This condition allows additional water to penetrate the pores during the test, which would have been partially filled before drying. As this method calculates density based on the displaced volume in a container, the presence of water in the pores influences the results because less volume is displaced by the beads. This leads to a lower measured volume of the beads and, as a result, the density becomes higher.

The results of these tests with equation 2.5 are shown in the table below (Tab.3.2).

	LECA	
	3/8 mm $[kg/m^3]$	8/20 mm $[kg/m^3]$
PDT1 - ρ_a	631,14	576,74
PDT2 - ρ_a	638,78	587,69
PDT3 - ρ_{rd}	647,07	597,67

Tab. 3.2: Particle density according to Archimedes principle.

3.3 Packing density

3.3.1 Packing measured using hardened concrete

All the results from both test experiments (Test T1 - cement & microsilica and test T2 - LC^{3}70) are presented in the following tables 3.3 and 3.4.

In test experiment T1 (cement & microsilica), three different bead size distributions were pumped. We started with 70% of 8/20 mm and 30% of 3/8 mm. Then, one tube was filled with

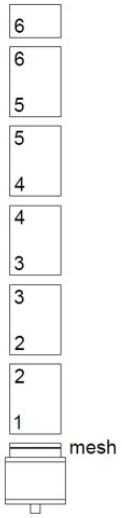

	LECA		
	70% - 8/20mm & 30%-3/8mm [%]	3/8 mm [%]	8/20 mm [%]
1-2 (15 cm)	59,6 ± 1	60,7 ± 0,9	59,5 ± 0,4
2-3 (15 cm)	59,2 ± 1	60,3 ± 0,9	59,2 ± 0,4
3-4 (15 cm)	59,3 ± 1	60,9 ± 0,9	59,6 ± 0,4
4-5 (15 cm)	60,2 ± 1	61,0 ± 0,9	59,9 ± 0,4
5-6 (15 cm)	61,8 ± 1	61,4 ± 0,9	60,3 ± 0,4

Fig. 3.3: Packing density of test 1 (T1).

only 3/8 mm, and finally, another tube was filled with only 8/20 mm. As shown in the table, for the first tube (70% – 8/20 mm and 30% – 3/8 mm), the following values were determined: the average packing density (PD) over the entire height is 60.2% ± 1. This density starts at 59.6% ± 1% at the bottom (Sections 1 – 2) and increases to 61.8% ± 1% at the top (Sections 5-6). The same trend of increasing packing density along the height can also be observed in the other two pumped tubes. In the case of 3/8 mm, an average PD of 60.9% ± 0.9% was achieved, and for the bead size of 8/20 mm, an average PD of 59.8% ± 0.4% was attained. The explanation for this change in density along the height can be attributed to the pressure applied to the aggregates from below. Since at the top of the pipe a lid needs to placed after filling it with the aggregates, a perfect filling of the beads is not possible. A air pocket forms underneath the lid. Therefore, when pressure is exerted from below, it could slightly alter the packing density in the upper part of the tube, since there is room for the beads to move upwards. After reaching the lid they get compressed and this could elevate the PD with increasing height, i.e. the beads rearrange during infiltration.

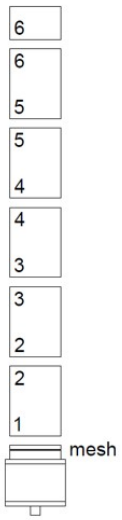

	LECA		
	70% - 8/20mm & 30%-3/8mm [%]	3/8 mm [%]	8/20 mm [%]
1-2 (15 cm)	59,4 ± 0,6	57,5 ± 1,2	57,9 ± 0,4
2-3 (15 cm)	59,2 ± 0,6	58,3 ± 1,2	57,9 ± 0,4
3-4 (15 cm)	59,5 ± 0,6	59,0 ± 1,2	58,0 ± 0,4
4-5 (15 cm)	60,5 ± 0,6	59,4 ± 1,2	58,7 ± 0,4
5-6 (15 cm)	60,5 ± 0,6	61,2 ± 1,2	58,8 ± 0,4

Fig. 3.4: Packing of test 2 (T2).

In test series T2 ($LC^3$70), the results with $LC^3$70 are extremely similar to the first test series. It should be noted that the packing density for the 70% – 8/20 mm and 30% – 3/8 mm mix ratio averages 59.8% ± 0.6% over the entire height, which is only 0.4% lower than in the results from T1. Similar, the value for the 8/20 mm bead size is 58.3% ± 0.4%over the entire height, and the values are also very similar over the individual sections. The only interesting difference in the second compared to the first test series is the slightly larger difference at 3/8 mm. A PD of 59.1% ± 1.2% was measured in T2, so the average density is 1.8% lower then in T1. The only explanation for this could be that this occurred during the filling of the Leca beads. The two bead sizes are first mixed in a bucket and then an attempt is made to fill them with a funnel. Since, as a rule, the larger particles rise to the surface and the smaller ones tend to sink, this could have led to some segregation in the individual parts, resulting in the deviation of just under 1.5%.

3.3.2 Packing with water

It is worth noting that the values obtained through this method are approximately 5% lower than those obtained using cement and photo analysis. The problem with this test method is the falsification due to the lower area of the setup, where the hose connection is placed on the tube. Due to a slight elevation on the inside, a little water always remains, and this cannot be measured accurately. Furthermore there is a lot of residual surface water on the beads, that can not be reliably measured. This analysis method is not particularly accurate or reliable, so it was not pursued further.

3.3.3 Packing measured using image analyse of sections of hardened concrete

The packing density was also investigated after the last two tests using the image analysis program ImageJ. For this purpose, all 3 cylinders resulting from infiltration experiment were cut into five 15 cm long sections and then photographed from both sides using appropriate lighting conditions. The ratio of the area of the leca beads to the total area was analyzed and calculated.

The results for packing density (see in table 3.3 and **??**) from Test 1 (cement & microsilica) are higher than those from Test 2 ($LC^3$70), as expected, after back-calculation over the packing with cement. On average, the following values were obtained for test 1: at 3/8 mm particle size 60.1% ± 1,3%, at 8/20 mm particle size 57.0% ± 1,9% and at 70% – 8/20 mm and 30% – 3/8 mm particle size 59.0% ± 2%.

As can be seen from these results, the 8/20 mm bead size has the lowest packing density, which could indicate that the voids between the individual beads have not been adequately filled or that the shape of the beads does not match as well as the other two bead sizes. Otherwise, we can think of no reason why the packing density of the three bead sizes should be different.

The results of the second test, as shown in table 3.4, were evaluated. Similar to T1, it can be seen that the 8/20 mm bead size has the lowest packing density with an average of 57,0 %. The other two bead sizes are almost equally distributed, with 3/8 mm having the highest density and 70% – 8/20 mm and 30% – 3/8 mm showing a slightly smaller difference. It is noteworthy that the values in this case are much closer to each other than for T1. The lower values could be due to the quality of the photos and their visibility. As with the previous tests, the beads were manually rearranged, which may lead to some variation in packing density. In the case of 70/30 mm, manual filling could also contribute to a reduction in packing density of around 2%.

A comparative analysis of both tests indicates that there is considerable potential to improve packing density. Further studies are required in this regard. Nevertheless, it can be concluded

T1: cement & microsilica			
	70% - 8/20mm & 30%-3/8mm [%]	3/8 mm [%]	8/20 mm [%]
1-2 (15 cm)	56,2 ± 2	58,1 ± 1,3	55,4 ± 1,9
2-3 (15 cm)	57,1 ± 2	59,3 ± 1,3	55,5 ± 1,9
3-4 (15 cm)	59,9 ± 2	60,0 ± 1,3	56,0 ± 1,9
4-5 (15 cm)	60,2 ± 2	61,0 ± 1,3	57,5 ± 1,9
5-6 (15 cm)	61,9 ± 2	62,0 ± 1,3	60,6 ± 1,9
Average	59,0 ± 2	60,1 ± 1,3	57,0 ± 1,9

Tab. 3.3: Packing density with Imagej T1.

that this method provides a comprehensive overview despite certain uncertainties, such as the difficulty in detecting the program edges around the beads. A possible improvement could be to increase the contrast, for example by coloring the Leca beads and the surrounding material.

T2: $L^3$70			
	70% - 8/20mm & 30%-3/8mm [%]	3/8 mm [%]	8/20 mm [%]
1-2 (15 cm)	54,1 ± 2,1	54,3 ± 2,3	53,3 ± 1,7
2-3 (15 cm)	55,9 ± 2,1	56,1 ± 2,3	56,9 ± 1,7
3-4 (15 cm)	56,5 ± 2,1	57,3 ± 2,3	57,2 ± 1,7
4-5 (15 cm)	58,6 ± 2,1	58,6 ± 2,3	57,5 ± 1,7
5-6 (15 cm)	60,6 ± 2,1	61,2 ± 2,3	58,0 ± 1,7
Average	57,2 ± 2,1	57,5 ± 2,3	56,6 ± 1,7

Tab. 3.4: Packing density with Imagej T2.

3.3.4 Packing density comparison

When looking at the three tests, there are differences in the results. However, it is important to note that all three test methods are different and can therefore have different error potentials. When determining the packing density by back-calculating using the weight of the Leca beads and the weight or density of the cement, there is a potential for error, as the water mass in the tube, due to pre-wetting, is unknown. An additional error could be that the weight of the Leca spheres is assumed to be evenly distributed over the sample. In contrast, image analysis, although providing reasonable accuracy, primarily examines the surface of the material and may overlook the changes within the material. In this way, the properties of the individual cut surfaces are also transferred to the height of the sample (15 cm), which can lead to a distorted results. As can easily be seen when comparing the back calculation method and the image analysis method in tab. 3.5,3.6 and 3.7, the deviation is most pronounced in the first 15 centimetres (the lower range of the infiltration height) for all three bead sizes. However, as the height increases, the deviation decreases to almost zero. This discrepancy between the two measurement methods could be due to deviations in the measurement methods, such as water in the pores not taken into account by pre-wetting in the back calculation or a bead in the photo analysis which is covered by a layer of cement, for example. However, these are only assumptions and therefore this comparison

requires further and more precise investigation. As already mentioned the water packing density test is not reliable. It is therefore not possible to say which of the three measurements used is the most accurate.

In summary:

- The packing density for all three bead sizes investigated is between 56% and 60%.
- Back calculation over the concrete may have errors due to water mass in beads from pre-wetting.
- The image analysis, where the contours were traced by hand, has a error rate.
- The analysis using water is falsified due to the setup and additionally difficult to measure, as water remains on the surface of the beads.

70% - 8/20 mm & 30%-3/8 mm			
T1: cement & microsilica			
section	back-calculation	image analyse	deviation
1-2 (15 cm)	59,6	56,2	3,4
2-3 (15 cm)	59,2	57,1	2,1
3-4 (15 cm)	59,3	59,9	-0,6
4-5 (15 cm)	60,2	60,2	0
5-6 (15 cm)	61,8	61,9	-0,1
T2: $LC^3$70			
section	back-calculation	image analyse	deviation
1-2 (15 cm)	59,4	54,1	5,3
2-3 (15 cm)	59,2	55,9	3,3
3-4 (15 cm)	59,5	56,5	3,0
4-5 (15 cm)	60,5	58,6	1,9
5-6 (15 cm)	60,5	60,6	-0,1

Tab. 3.5: Comparison PD of 70% - 8/20 mm & 30%-3/8 mm.

3/8 mm			
T1: cement & microsilica			
section	back-calculation	image analyse	deviation
1-2 (15 cm)	60,7	58,1	2,6
2-3 (15 cm)	60,3	59,3	1,0
3-4 (15 cm)	60,9	60,0	0,9
4-5 (15 cm)	61,0	61,0	0
5-6 (15 cm)	61,4	62,0	-0,6
T2: $LC^3$70			
section	back-calculation	image analyse	deviation
1-2 (15 cm)	57,5	54,3	3,2
2-3 (15 cm)	58,3	56,1	2,2
3-4 (15 cm)	59,0	57,3	1,7
4-5 (15 cm)	59,4	58,6	0,8
5-6 (15 cm)	61,2	61,2	0

Tab. 3.6: Comparison PD of 3/8 mm.

8/20 mm			
T1: cement & microsilica			
section	back-calculation	image analyse	deviation
1-2 (15 cm)	59,5	55,4	4,1
2-3 (15 cm)	59,2	55,5	3,7
3-4 (15 cm)	56,6	56,0	0,6
4-5 (15 cm)	59,9	57,5	2,4
5-6 (15 cm)	60,3	60,6	-0,3
T2: $LC^3$70			
section	back-calculation	image analyse	deviation
1-2 (15 cm)	57,9	53,3	4,6
2-3 (15 cm)	57,9	56,9	1
3-4 (15 cm)	58,0	57,2	0,8
4-5 (15 cm)	58,7	57,5	1,2
5-6 (15 cm)	58,8	58,0	0,8

Tab. 3.7: Comparison PD of 8/20 mm.

3.4 Injection test series with cement & microsilica

The path to the first successful test experiment, using 100% of 3/8 mm, 100% of 8/20 mm beads, as well as the combination of 70% – 8/20 mm and 30% – 3/8 mm. Prior to this, a total of 22 experiments were necessary to establish both a functional setup and a well-functioning slurry. A comprehensive list of the preceding experiments is available in the appendix.

For the first experiment with beads, we once considered the three different bead size distributions and attempted to inject them. We followed the same procedure as described in section 2.2.1 to create the slurry for each attempt. Additionally, the same steps were carried out for each pumping trial. First, the mixture was prepared, then a funnel test and a spread test were conducted. Afterward, the mass was loaded into the pump and injection test started.

Based on our past experiments, we knew that the pressures generated when pumping the 8/20mm bead size were not particularly high. Therefore, we used a transparent plexiglass tube be able to see what is happening inside the pipe during the pumping process and measure the infiltration pace of the slurry over the height. Before starting the injection, the beads were pre-wetted, as this was a crucial step to prevent slurry blockage. This information derived from previous trials and other studies. In the other two experiments, we used the orange PVC tubes because higher pressures were generated, and in other tests often the plexiglass pipe was crushed.

During the pumping process, the following observations were made:

Due to pre-wetting, there was always some water left at the bottom at the transition piece because of the small elevation for the hose connection. This resulted in the initial upward movement of all the water from the bottom was pumped upwards as seen in figure 3.5. Subsequently, the slurry was immediately pumped up. It was noticeable that some additional water stored by the beads was also transported upward during the process. As clearly visible in the following picture 3.5b, there is still clear water at the bottom, and as it rises, there is mixing of slurry and water occurring, causing it to appear cloudy (Figure 3.5a).

(a) Cloudy water. **(b)** Clear water.

Fig. 3.5: Visualization of different types of water in a pipe.

Furthermore, it was observed that all experiments with the larger beads exerted almost no additional pressure on both the pump and the pressure sensor attached to the tube. Here, the hydrostatic pressure was the predominant force.

In all three experiments, we managed to reach the upper end of the tube, which meant we were able to pump through approximately 85 cm of beads. We kept the recipe for the slurry largely the same for all three bead sizes, except for one exception with the ratio of 70% 8–20 mm and 30% 3–8 mm. Since the other two ratios worked without any issues, we decided to use slightly less superplasticizer and retarder.

In each pumping attempt, we tried to pump the slurry until nearly identical slurry emerged at the upper end of the tube as was initially pumped in at the bottom. Originally, this mixture was heavily diluted with water and it typically took 3-5 minutes to get nearly the same constancy. After pumping, we only conducted another spread test. As shown in table 3.8, the following parameters were used for the tests.

SP	superplasticizer
Sky	retarder

T1: cement & microsilica								
Leca [mm]	w/c [-]	cement [kg]	microsilica [kg]	SP [g]	Sky [g]	spread [cm]	funnel [s]	Yiel stress [Pa]
3/8	0,35	12,00	1,20	50	25	22,40	1,56	24,06
8/20	0,35	12,00	1,20	62	31	22,50	1,38	23,53
70% - 8/20 & 30%-3/8	0,35	12,00	1,20	62	31	21,50	1,71	29,37

Tab. 3.8: Test parameter T1.

3.4.1 Pressure measurements

In all test experiments, we closely monitored pressure for both, tube sensor and pump. As clearly visible in the three figures, when using the 8/20 mm bead size, only about 1 bar pressure was measured on the sensor, and there was no pressure indicated on the pump. This tends to show infiltration with the slurry is easily achievable. Confirmed by all preliminary tests larger bead sizes never caused any issues. The infiltration rate is a critical parameter in understanding infiltration processes, as it indicates how well a slurry can penetrate a bed of beads. We were only able to measure the infiltration rate in one test, as we used a transparent tube only for that particular experiment, which was test T1 (cement & microsilica) with 8/20 mm beads. As mentioned earlier, this test exhibited very low pressures. In the other tests, we used orange PVC tubes because they could withstand higher pressures.

In the test T1, we measured an infiltration rate that began at a low speed pump rate of 0.312 l/min. Upon reaching the top, a nearly identical flow rate of 0.298 l/min was measured. As depicted in figure 3.6, the pressure curve is almost linear, resulting in a constant increase in pressure

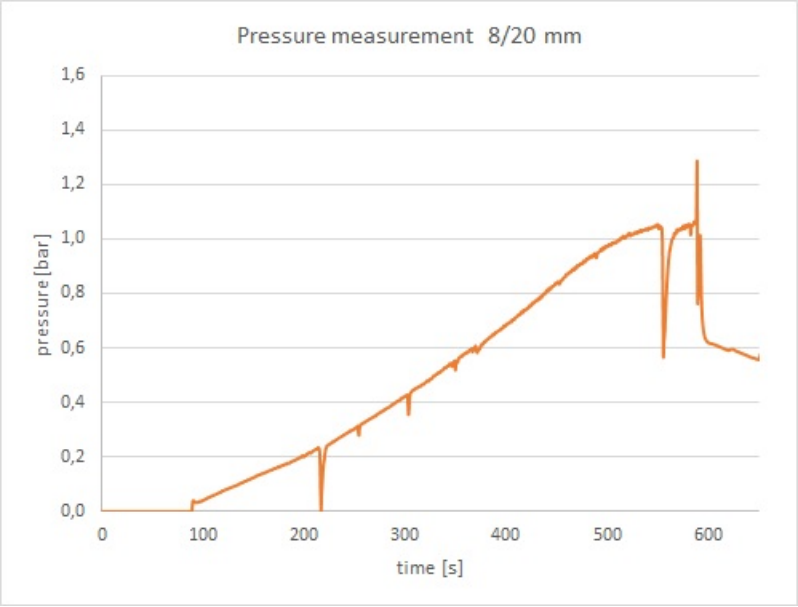

Fig. 3.6: Pressure measurement 8/20 mm T1.

In the case of the test with 3/8 mm bead size, a significant increase in the pressure compared to the previous test is observed. The pressures measured here reach up to 7.8 bar on the pressure sensor before reaching the upper edge of the pipe. Unfortunately, in this case, it was not possible

to determine a flow rate as the slurry arriving at the top was initially too watery. Towards the end of the experiment, we had to terminate it for safety reasons when the pump reached almost 20 bar of pressure before the desired consistency of slurry arrived at the top.

During this test run, we only measured the pressure curve (fig.3.7), which in the first 400 seconds rises very slowly and follows a very linear pattern. However, from around 420 seconds upwards, the pressure increases rapidly and resembles an exponential function. There are two possible explanations for this rapid pressure increase. One possibility is that there was a blockage in the area of the sensor, causing the slurry to be pressed into the pipe without moving further upwards. Another hypothesis could be that the presence of a lid at the top, even though it has the same cross-section as the inlet at the bottom, may have obstructed the passage of the slurry, possibly due to beads narrowing the cross-section. This could have led to an increase in pressure in the pipe.

Since all of these are speculative explanations, further investigations are required.

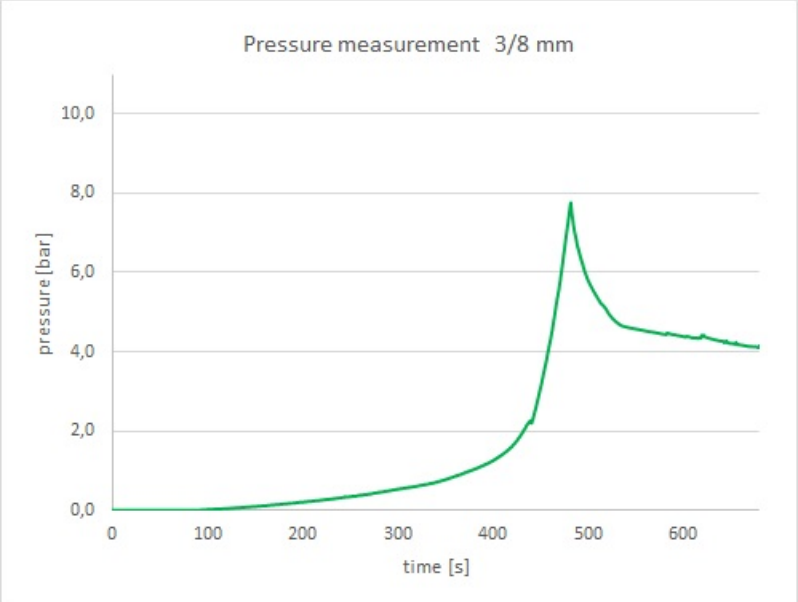

Fig. 3.7: Pressure measurement 3/8 mm T1.

In the test run with 70% – 8/20mm & 30% – 3/8mm beads (Fig. 3.8), a nearly identical pattern to the test with 3/8 mm bead size was observed. However, the pressure curve increased even more rapidly at a certain point, reaching a maximum of up to 10.14 bar. It is also evident from the graph that the measurement abruptly ended when the pump pressures reached their maximum. The reasons for this rapid increase can only be speculated upon, similar to the 3/8 mm test, and further investigations are required.

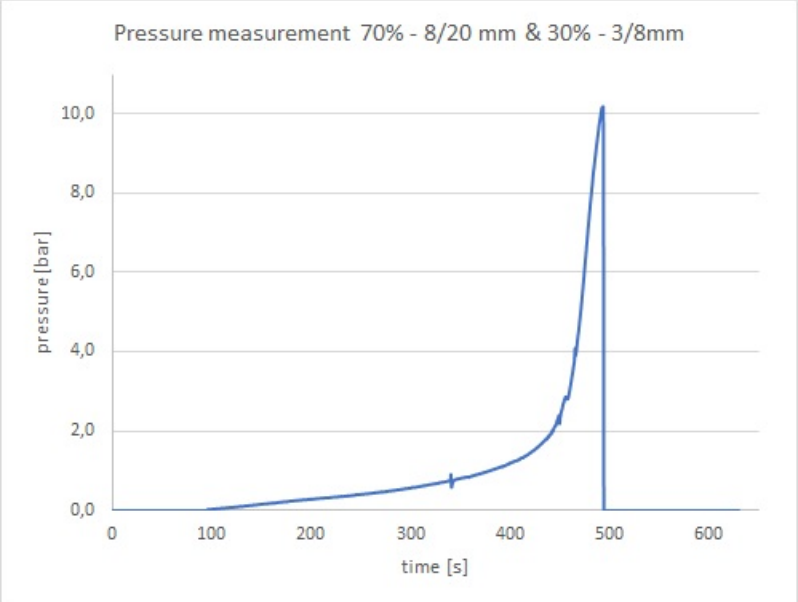

Fig. 3.8: Pressure measurement 70% – 8/20 mm and 30% – 3/8 mm T1.

3.4.2 Density of the hardened concrete

The densities of the individual 15 cm samples were measured and are listed in table 3.9. Regardless of the bead size, the densities are all between 1100 kg/m³ and 1200 kg/m³. Conventional concrete has a bulk density of 2500 kg/m³, which makes the developed concrete half as light. As can be seen in figure 3.9, the density increases slightly for all three bead sizes between sections 2 and 4. However, the trend line over the height shows that the density becomes lighter towards the top. As already explained, this could be due to factors such as the packing density. Due to the infiltration from below and the force acting on the beads, more beads are pushed upwards, resulting in less cement. This also explains the increase in packing density in section 3.3.4. To better control the distribution, the packing density should possibly be further optimized to minimize displacements of the beads.

Density of the hardened samples T1: $L^3 70$			
	70% - 8/20mm & 30%-3/8mm $[kg/m^3]$	3/8 mm $[kg/m^3]$	8/20 mm $[kg/m^3]$
1-2 (15 cm)	1194,2	1171,6	1188,8
2-3 (15 cm)	1207,1	1181,4	1198,7
3-4 (15 cm)	1209,9	1191,3	1166,5
4-5 (15 cm)	1177,4	1181,2	1167,2
5-6 (15 cm)	1129,4	1169,3	1147,4

Tab. 3.9: Density of the hardened samples T1.

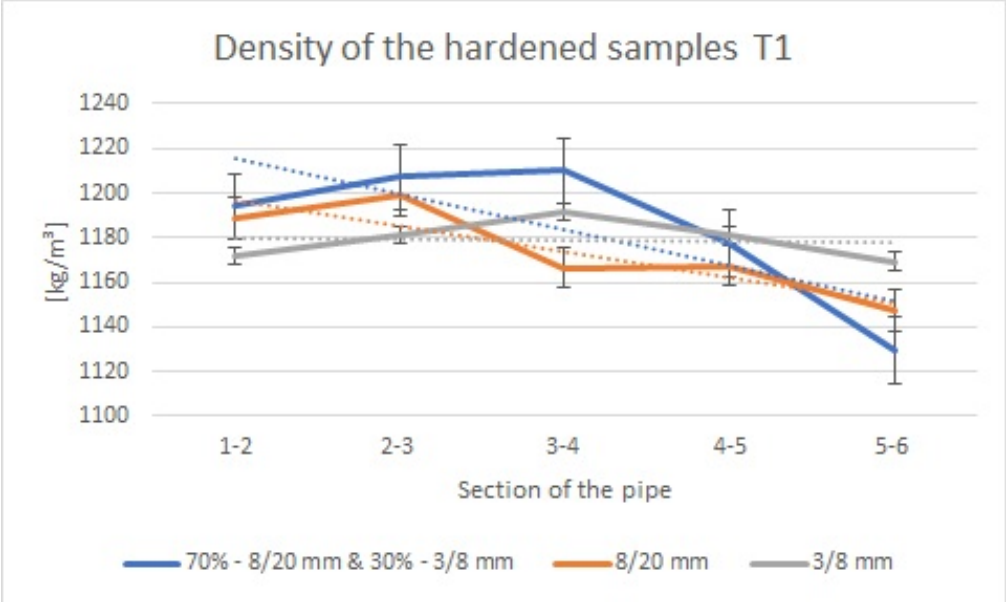

Fig. 3.9: Density of the hardened concrete T1.

3.4.3 Compressive strength

Additionally, we tested the slurry without beads and achieved an average of three compressive strength tests (Fig.2.24) value of 91.3 MPa from three trials. The results for the individual sections of the samples can be found in figure 3.10, ranging between 10 and 13 MPa. The measured values for compressive strength are in the lowest range compared to lightweight concrete (LC12/13), as described in Chapter 2.2.9.2. The results show only about one third of the compressive strength compared to the conventional use of concrete with class C25/30. Therefore, this type of concrete is only suitable for larger components to meet the necessary strength requirements. To achieve better compressive strength, a method would have to be developed to mitigate the filtration of cement slurry into the beads and the water content using the pre-saturation of the beads, which could improve the overall strength of the matrix. The increase of the particle density could also have a positive effect on increasing the compressive strength. Nevertheless, it should be noted that the Leca beads can never achieve the same strength values as conventional aggregates. However, achieving more compressive strength might be possible.

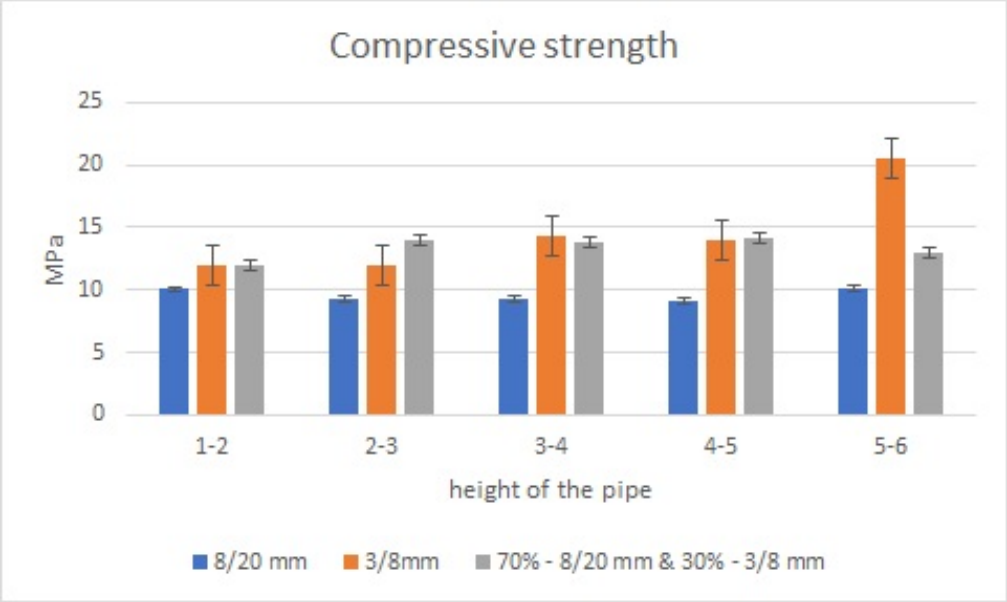

Fig. 3.10: Compressive strength T1.

3.4.4 Thermal conductivity

For each sections between the samples three tests per surface were conducted, and an average of these was calculated. As visible in figure 3.11, the values fluctuate over the height of the tube. As observed, the thermal conductivity decreases with increasing height. This phenomenon can be attributed to the rising packing density, as elaborated in section section 3.3.4. Additionally due to rotation of the samples during testing, the sensor could be in direct contact with only beads or only cement slurry potentially leading to vastly different thermal conductivity and possibly affecting the test results.

The 8/20 mm beads show an average thermal conductivity of 0.50 W/mK, the 3/8 mm beads have an average of 0.55 W/mK, and the 70% – 8/20 mm and 30% – 3/8 mm mixture registers 0.53 W/mK on average. These values align well with the corresponding bulk density of the samples, as seen in figure 3.11 and are consistent with DIN 4108.

When trying to identify a correlation between density (see fig. **??** and thermal conductivity, no clear increase can be seen. Even when using a best-fit line, it is not possible to make a precise statement about how the density affects the thermal conductivity of these samples and vice versa. There are very strong outliers here and the possible reason for this may be the measurement method using the hot disk.

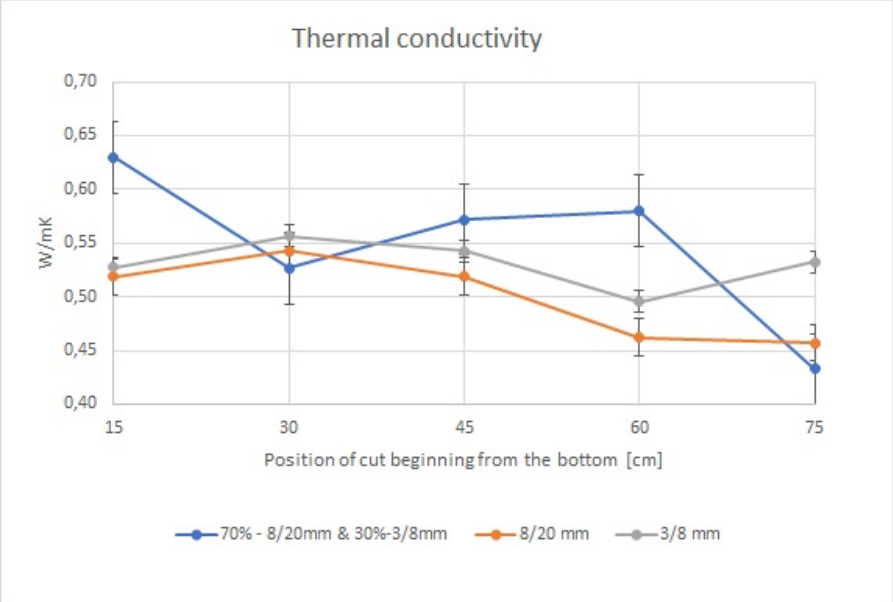

Fig. 3.11: Thermal conductivity test T1

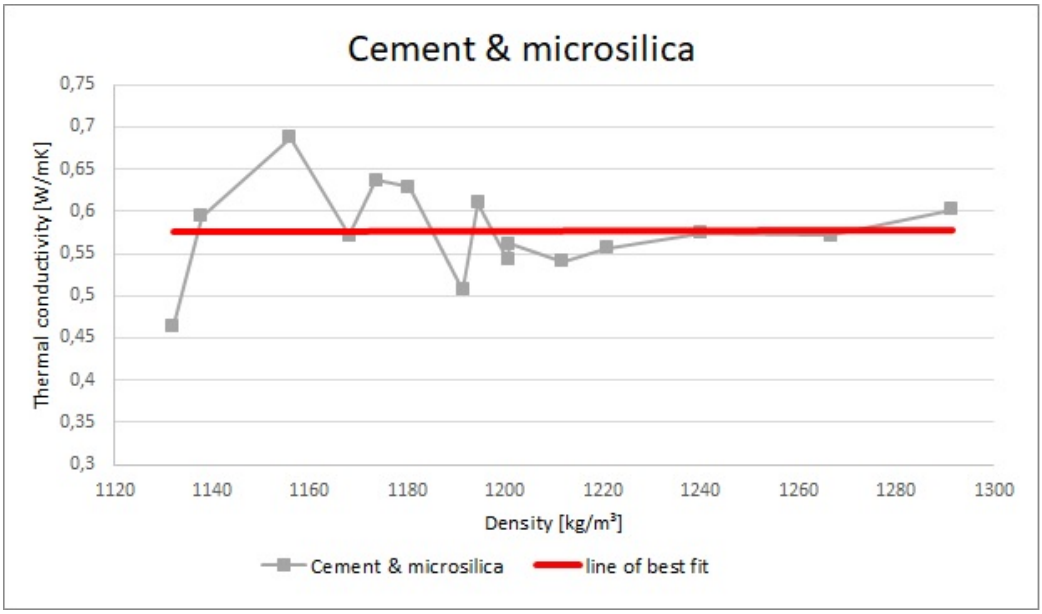

Fig. 3.12: Correlation thermal conductivity and density T1.

3.5 Injection test series with LC^{3}70

To create an LC^3 mixture suitable for the pump test. For this, we needed to determine the appropriate water to binder (w/b) ratio for the mixture and the right amounts of superplasticizer and retarder. We mixed LC^{3}55 and LC^{3}70 in a container and conducted multiple spread tests with different mixtures, adjusting the amounts of superplasticizer and retarder to achieve both a similar visual consistency as in T1 (Injection with cement & microsilica) and a comparable spread distance using the spread test. As shown in table 3.10, the following parameters were used for the tests.

T2: LC^{3}70										
Leca [mm]	w/c [-]	cement [kg]	CC [kg]	LS [kg]	water [l]	SP [g]	Sky [g]	spread [cm]	funnel [s]	Yield stress [Pa]
3/8	0,35	11,2	4,00	0,80	5,60	78,64	33,32	26,80	1,66	9,52
8/20	0,35	11,2	4,00	0,80	5,60	78,64	33,32	26,50	1,79	10,07
70% - 8/20 & 30%-3/8	0,35	11,2	4,00	0,80	5,60	78,64	33,32	27,30	1,39	8,68

Tab. 3.10: Test parameter T2.

CC calcined clay
LS limestone
SP superplasticizer
Sky retarder

3.5.1 Pressure measurements

In Test 8/20 mm, we observed a nearly linear increase in pressure, reflecting the pressure of about 1 bar (see fig. 3.13). This implies that the slurry passed through the voids within the setup without resistance. The only slight pressure increase occurred around the 1150-second mark when the slurry reached the lid. This transient increase was due to the reduced cross-section caused by the presence of Leca beads in the hose at the lid. Furthermore, it was feasible to conduct a spread test that revealed a spread of 26.40 cm. This result demonstrates that, after flowing through or circulating within the setup, the slurry's properties remained constant.

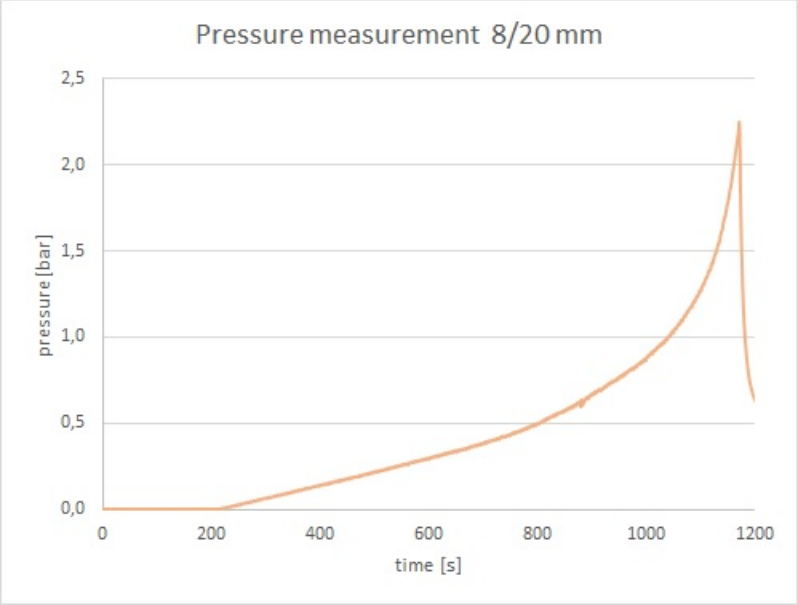

Fig. 3.13: Pressure measurement 8/20 mm T2.

In test 3/8 mm, we observed a linear increase in pressure (see fig. 3.14) followed by a sudden exponential increase that led to a temporary stop of the pump at around 13 bar. Despite a drop in pressure between 1000 and 1160 seconds, we continued the test and reached the highest

point where the sludge came out. However, due to the high pump pressure, we stopped before complete discharge and found a diluted sludge (see fig.3.15) at the top during disassembly. This anomaly could be due to a blockage in the lower pipe, which hindered further pumping.

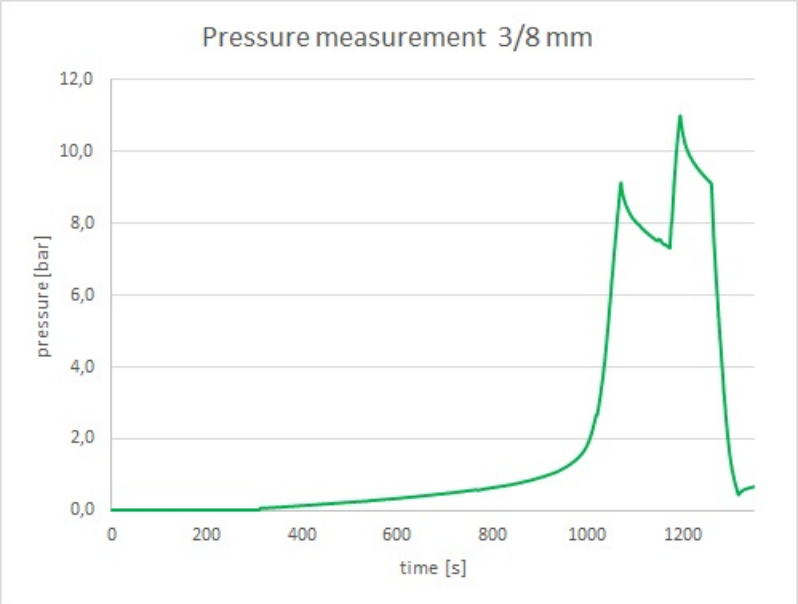

Fig. 3.14: Pressure measurement 3/8 mm T2.

Fig. 3.15: Dilution of test series 2 – 3/8mm LC[3].

In the 70% – 8/20 mm and 30% – 3/8 mm test of test series 2, the experiment proceeded without any problems, much like the 8/20 mm test. However, a measurement error occurred with the sensor, rendering the values in fig. 3.16 inaccurate. Importantly, during the experiment, we did not encounter any issues with the pump's pressure. Therefore, we didn't need to abort the test. This allowed the slurry to reach the top, and after allowing the slurry to run through briefly, we obtained sufficient mass for conducting the spread and funnel tests. The results revealed

that the spread was 25.30 cm, while the funnel test showed a time of 2.31 seconds. Interestingly, when comparing these figures to those in table 3.10, we observed that the spread had decreased by 2 cm from 27.30 cm, but the funnel time had increased from 1.29 seconds to 2.31 seconds. This change is intriguing, although we currently lack an explanation for it.

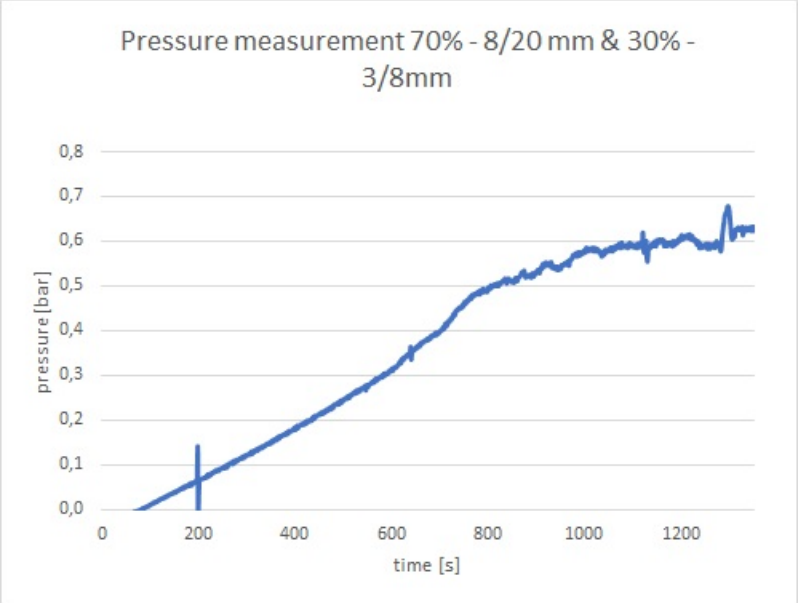

Fig. 3.16: Pressure measurement 70% 8/20 mm and 30% 3/8 mm T2

3.5.2 Density of the hardened concrete

The densities of the samples for the second test, regardless of the bead size, are listed in the following table 3.11. Similar to T1, the weight of the individual samples is in the range between 1100 kg/m³ and 1300 kg/m³. A slightly higher density in the samples of size 3/8 mm could be due to the fact that the beads were pushed upwards here, which would also explain the increased weight in the lower area (section 1-2), as there is more slurry than beads here. Figure 3.17 also clearly shows that the trend decreases with height and therefore the density decreases with height. Further investigations are required to achieve an improvement or constant density over the entire height.

Density of the hardened samples T2: L^{3}70			
	70% - 8/20mm & 30%-3/8mm $[kg/m^3]$	3/8 mm $[kg/m^3]$	8/20 mm $[kg/m^3]$
1-2 (15 cm)	1173,5	1291,49	1220,7
2-3 (15 cm)	1180,2	1266,62	1194,4
3-4 (15 cm)	1168,2	1240,1	1211,74
4-5 (15 cm)	1155,9	1200,7	1200,7
5-6 (15 cm)	1137,9	1131,9	1191,4

Tab. 3.11: Density of the hardened samples T2.

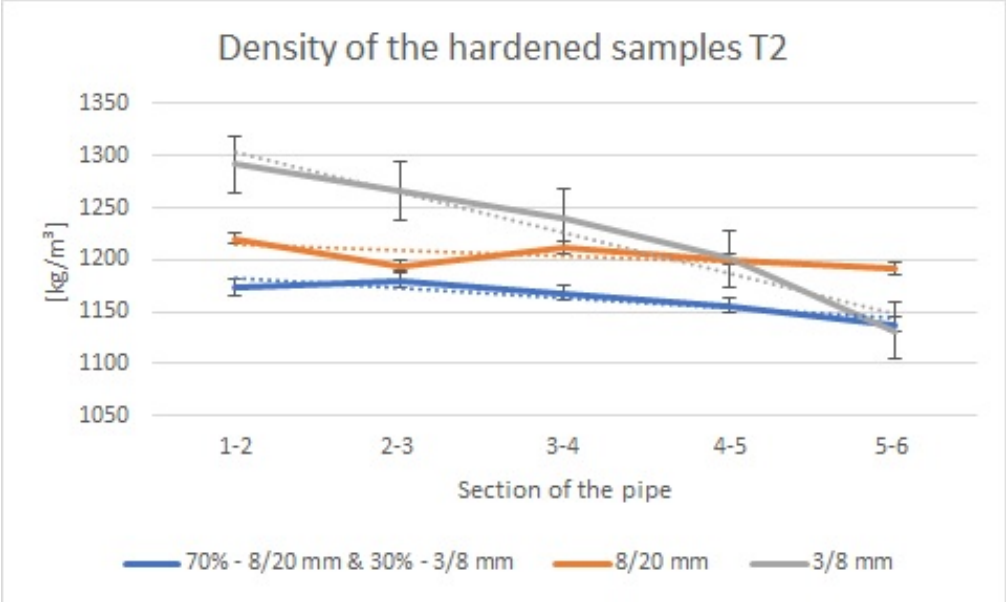

Fig. 3.17: Density of the hardened concrete T2.

3.5.3 Compressive strength

The results obtained from the compressive strength tests within test series 2 exhibit similarities to those of test series 1, albeit with a slightly higher range. The average values across all experiments fall within the range of 11 to 14 MPa (see fig. 3.18), representing an improvement of approximately 2 MPa compared to test series 1. While these values still fall short of the standards for typical concrete, they underscore a noteworthy enhancement in performance. However, achieving equivalence with conventional concrete necessitates further refinement. Utilizing this composition as a substitute for regular concrete remains contingent on precise and well-considered applications. The marginal improvement in compressive strength results can be attributed to refinements in the testing procedures themselves. Building on our experience with test series 1, we opted to perform surface grinding, resulting in improved contact with the testing apparatus and potentially contributing to these superior outcomes. Notably, this composition significant advantage lies in its reduced cement content, making it more environmentally friendly while maintaining a consistent level of compressive strength. For comparison, the values for the slurry only are 81.3 MPa. This reduction in relation to T1 can be attributed to the composition of the $LC^3$70 mixture.

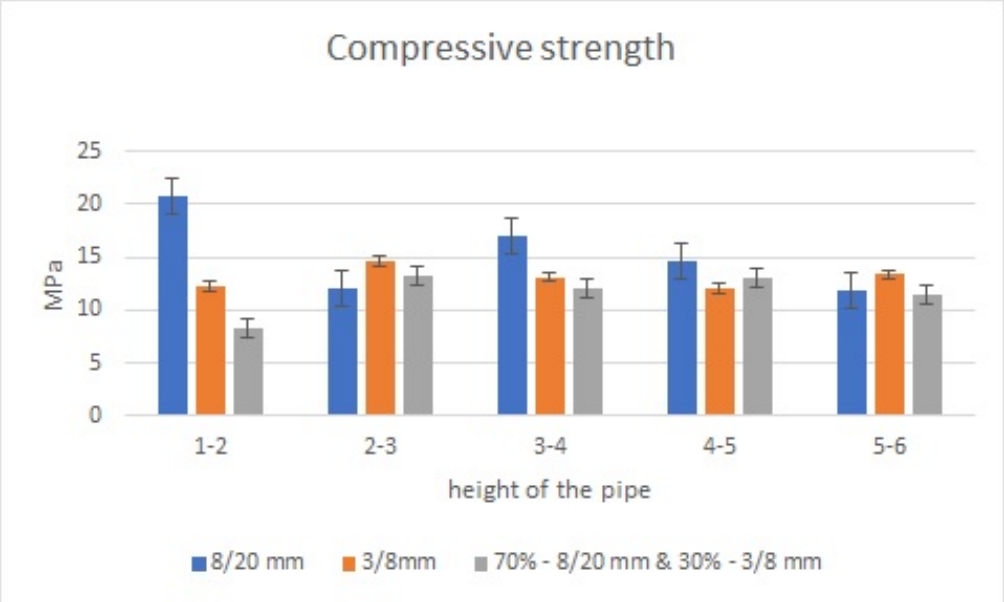

Fig. 3.18: Compressive strength T2.

3.5.4 Thermal conductivity

The measured values of test series 2 are slightly worse than those of test series 1, but when compared with the results of the cement-only test, it can be seen that cement with microsilica has a thermal conductivity of 1.04 W/mK, while the samples with LC^{3}70 show an average thermal conductivity of 1.12 W/mK. These results are difficult to explain. We assume that the slurry with LC^{3}70 has a worse effect on thermal conductivity because the thermal conductivity of cement is lower than that of the materials used in LC^{3}70. This discrepancy needs further investigation. The slightly higher thermal conductivity observed in the tests should be acceptable in view of the minimal deviation, as this is nevertheless a more environmentally friendly choice of material compared to the use of pure cement.

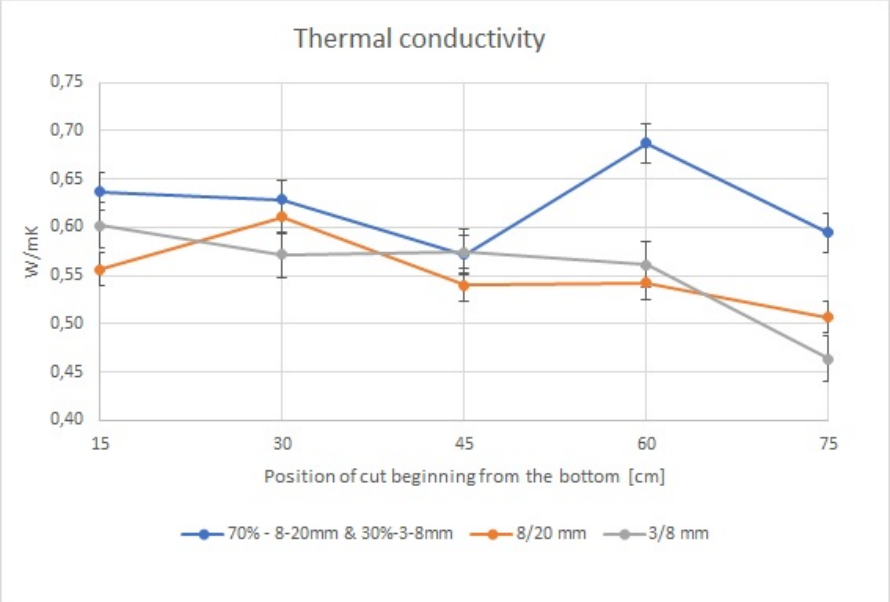

Fig. 3.19: Thermal conductivity test T2.

As can be seen in figure 3.20, there is a correlation between density and thermal conductivity in this test series. As the density increases, the values for thermal conductivity deteriorate. This observation could provide an explanation for the declining proportion of Leca beads. However, it should be noted that these values show some outliers, which puts the statement into perspective somewhat.

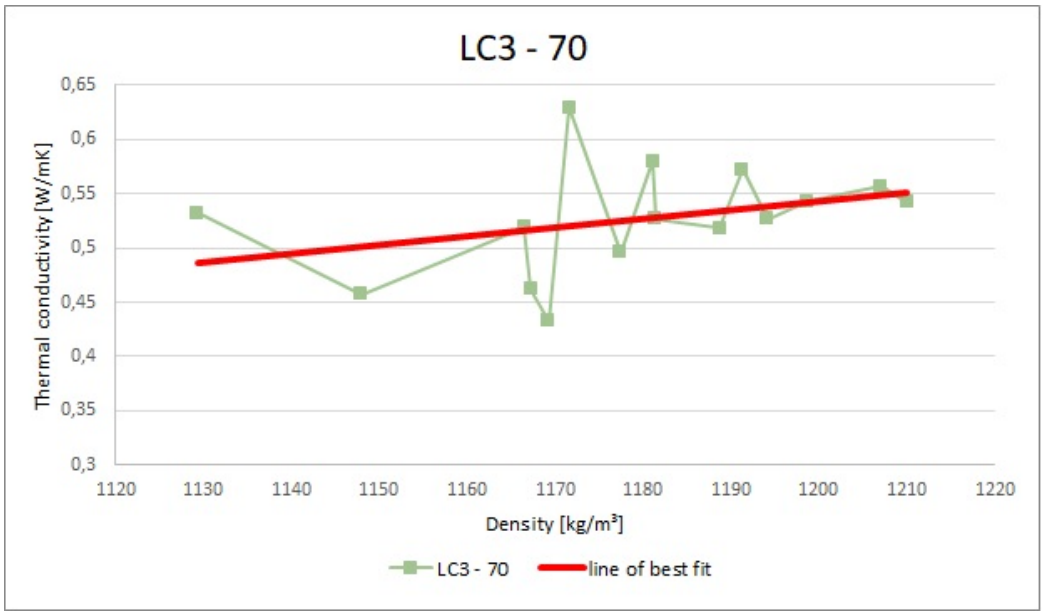

Fig. 3.20: Correlation thermal conductivity and density T2.

Chapter 4

Conclusion

This master's thesis represents a continuation of the work initiated by Lukas Pointnter [34]. Building upon the research conducted by Pointnter, this thesis delves into the critical aspects of infiltration. Specifically, it emphasizes the essential role of pre-wetting Leca beads to facilitate efficient infiltration and prevent the formation of pasty plugs. Pointnter's work highlights the advantages of bottom-up infiltration, which ensures uniform infiltration and higher packing density, albeit at the cost of increased labor input. Subsequent research endeavors are geared toward refining the composition of the cement slurry by adjusting the water-cement ratio and PCE content to enhance permeability and mitigate segregation during the infiltration of porous media. The principal focus of this study revolves around the development of a functional injection system for Leca beads. To this end, 22 different experimental setups were explored, with incremental adjustments aimed at determining the set up that can resist the highest pumping pressure. While some of these experiments yielded positive results, challenges arose when dealing with smaller particles because higher pressures are needed, particularly those measuring less than 3 mm. The primary issue encountered was the inability to achieve the intended infiltration, as each attempt resulted in a plug forming at approximately 15 cm within the bead structure. Leveraging insights from prior research, the study delved deeper into various aspects, including slurry composition optimization and the application of the bottom-up infiltration technique.

The findings from these tests offer critical insights. Notably, it appears that the lower section of the setup is capable of withstanding pressure, while potential issues may reside in the region just upstream of the mesh, especially near the sensor. Many instances where tests were halted were marked by the formation of a pasty layer, akin to a plug.This indicates that the challenges in this particular area persist, especially in those areas that are significantly influenced by the cement flow. Furthermore, the tests underscore the significance of pre-wetting the beads for successful infiltration over the entire height.

In summary, despite advancements in establishing an effective setup for particle sizes exceeding 3 mm and formulating a more environmentally friendly slurry, the research has yet to attain the desired level of compressive strength.

The achieved compressive strength remains significantly lower than that of conventional concrete, approximately one-third of the desired compressive strength.

Thermal conductivity, a parameter primarily dependent on density within the ranges specified in DIN 4108, also warrants attention. There is room for improvement in this regard through the optimization of packing density. Enhanced thermal conductivity holds particular importance in the context of improving the energy efficiency of buildings and reducing energy consumption.

Furthermore, the experiments reveal a consistent increase in packing density with height. Given that the beads were not effectively compacted by vibration, there is potential for further enhancement in future experiments. These outcomes contribute to a deeper understanding of Leca infiltration and lay the groundwork for future research in this domain.

Taken together, these results, in conjunction with the positive attributes of an improved CO2-adapted slurry and insights from prior research, underscore the need for continued efforts

and research to enhance the performance of this innovative material and expand its potential applications within the construction industry. The path forward lies in fine-tuning mix ratios, optimizing packing density, and devising methods to increase compressive strength while reducing thermal conductivity. The intricate interplay between these parameters demands further optimization.

Appendix

So far, it has not been possible to pump out a smaller grain size than 3-8 mm. This resulted in either a failure of the setup due to reaching the maximum pump pressures or one of the components in the setup couldn't withstand the forces and pressures involved.

1. Preliminary tests

Other used materials: To test the system and avoid wastage of materials, we used an older cement, namely CEM II/B 32.5 R(Fig. 4.1)

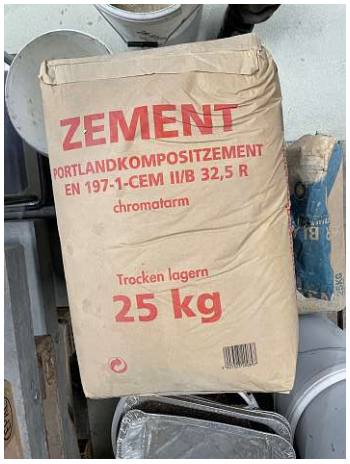

Fig. 4.1: CEM II/B32,5 R.

Test 0.1: In this experiment, we assembled the initial set-up and attempted to pump the three different aggregates with sizes of 1/4, 4/8, and 8/16 mm using water only.

Test 0.2: In this experiment, a slurry was prepared using only CEM II with a water-to-cement w/c ratio of 0.40% (see lable 4.1. It was possible to pump the 8/16 aggregate successfully. For the 4/8 aggregate, although we reached the upper edge, cement slurry was squeezed out between the funnel and the pipe due to higher pressures. The 1/4 system failed because the hose slipped off the funnel (Fig. 4.2).

Aggregates [mm]	w/c [%]	pre wetted [-]	spread [cm]
1-4,4-8,8-20	0,40	no	12,80

Tab. 4.1: Test parameters test 0.2.

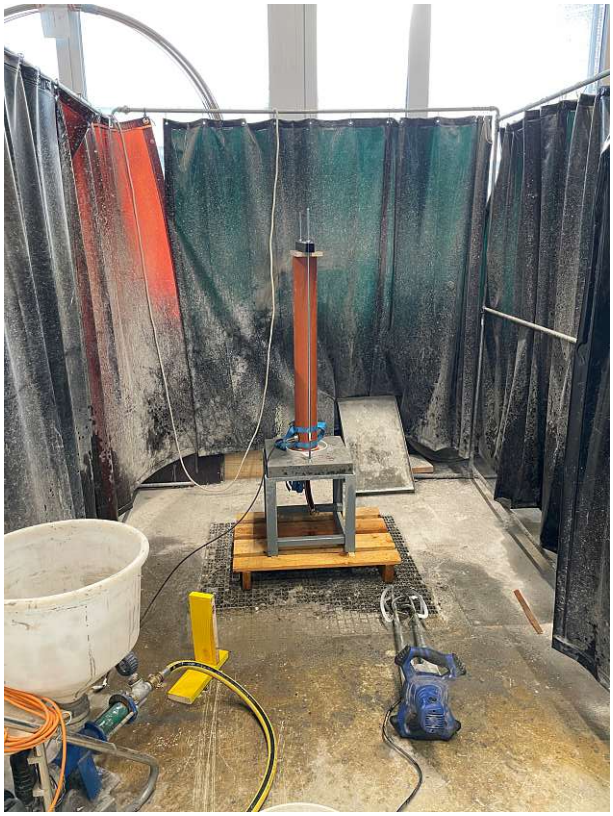

Fig. 4.2: Test attempt 0.2.

Test 0.3: In this experiment, is the same as Test 0.2, but 0.1% superplasticizer was added (table 4.2). The only reason for the system's failure at 1/4 was that the bottom cover broke when it reached 20 bar of pressure at the pump. When we examined the material, we noticed that when pumping 1-4 mm, the mixture in the hose still had the same consistency as when it was initially poured, but within the aggregates, the material was very stiff and almost solid.

Aggregates [mm]	w/c [%]	Ace 430 [%]	pre wetted [-]	spread [cm]
1/4,4/8,8/20	0,40	0,10	no	14,9

Tab. 4.2: Test parameters test 0.3.

Fig. 4.3: Test attempt 0.3.

Test 0.4: Test 0.4 was the same as Test 0.3, but we increased the amount of superplasticizer from 0.1% to 0.2%, resulting in a higher spread. Additionally, in the first 15 cm, we used 8/16 aggregates to reach the pressure sensor. This was done because if a plug occurred before the sensor, we wouldn't be able to observe what was happening at the sensor.

The problem in this test was similar to the previous one. We were unable to reach the top, and this time, the material in the hose appeared to be squeezed out as if the pressure had removed the water from the slurry. In the lower section (8/16), the slurry was completely stiff, similar to what was observed in the hose. However, in the section above (1/4), it remained almost identical to its state after mixing.

Aggregates [mm]	w/c [%]	Ace 430 [%]	pre wetted [-]	spread [cm]
1/4	0,40	0,20	no	23,80

Tab. 4.3: Test parameters test 0.4.

Fig. 4.4: Test attempt 0.4

Test 0.4.1: In this experiment, the only modification was made in step 0.4, which involved washing and pre-wetting the aggregates. However, despite this adjustment, which allowed a greater infiltration height of 8 cm than before, the result was unsuccessful because a plug formed and the soil cover broke.

Aggregates [%]	w/c [%]	Ace 430 [%]	pre wetted [-]	spread [cm]
1/4	0,40	0,20	yes	23,80

Tab. 4.4: Test parameters test 0.4.1.

Fig. 4.5: Test attempt 0.4.1.

Test 0.5: Test 0.5 was the same as test 0.4 , but we increased the amount of superplasticizer to 0.3%. For this test, we used the information from the previous tests and slightly reduced the water content before trying it again to w/c=0,3. We also extended the set-up to include 4 rods. We made some changes both at the bottom and the top. At the top, we now have a four-sided attachment, replacing the previous two-sided one. There is also a cross-like structure at the top to hold down the pipe. At the bottom, we removed the wooden plate and attempted to pump the slurry directly onto the UHPC (Ultra-High-Performance Concrete) plate.

However, the system failed again, this time at the bottom.

Aggregates [mm]	w/c [%]	Ace 430 [%]	pre wetted [-]	spread [cm]
1/4	0,30	0,30	yes	26,50

Tab. 4.5: Test parameters test 0.5.

Fig. 4.6: Test attempt 0.5.

Test 0.6:
In this test, we added 22.5 g of sugar to slurry as a retarder. The test failed because of a plug directly behind the sensor.

Aggregates [mm]	w/c [%]	Ace 430 [%]	pre wetted [-]	spread [cm]
1/4	0,30	0,35	yes	20,80

Tab. 4.6: Test parameters test 0.6.

Test 0.6.1: In this test, unlike the previous one, we reduced the amount of sugar to 18g and tried the test again. Once again, a plug occurred near the sensor.

Aggregates [mm]	w/c [%]	Ace 430 [%]	pre wetted [-]	spread [cm]	funnel [s]
1/4	0,50	0,0	yes	29,5	1,10

Tab. 4.7: Test parameters test 0.6.1.

Test 0.7: The attempt with the expanded clay beads 1/3 mm we had to interrupt, because the pump indicated at 20 bar and this had the maximum pressure load for the hose. When checking the problem, a plug again appeared downwards at the mesh.

Aggregates [mm]	w/c [%]	Ace 430 [%]	pre wetted [-]	spread [cm]	funnel [s]
1/3	0,35	1,19	yes	24,0	1,56

Tab. 4.8: Test parameters test 0.7.

Fig. 4.7: Consistence of slurry.

Fig. 4.8: Different consistence in the pipe.

Fig. 4.9: Material downwards the mesh.

Test 0.8: For test experiment 0.8, we attempted only one trial. Another master's student had prepared a mixture with UHPC and this mixture was very fluid. So we wanted to test how far we could let it penetrate into a pipe filled with normal aggregates using gravity and a vibrating plate. In Fig.4.10 you can see that we only reached 2/3 of the height. For this mixture we used the following mix (see fig. 4.11).

Fig. 4.10: Test attempt 0.8.

Neue Mischungsberechnung für UHPC V2015-01-29

durchgeführt von:	Dr. Johannes Kirnbauer	Ort:	Labor 1030, Lilienthalgasse 14	Datum:	05.09.2023
Zweck:	**CEM III 0,25 10KSM**				

◊ Grau hinterlegte Felder müssen eingetragen werden ◊

Anforderungen		**Kennwerte**			
W/Z-Wert	0,250	W/B-Wert (C+Zus.reaktiv)	0,250	Fließmittel [M% v. F]	0,91
Sand trocken [dm³/m³]	350,00	W/Fv-Wert	0,651	Relativdichte rechnerisch	0,821
Luftgehalt (angenommen) [V.%]	2,00	PD	74,666	Fließmittel [V% v. Fv]	2,39

Matrix

	Bezeichnung	Anteile [M. 1]	Anteile [V. 1]	Masse [kg]	Rohdichte [kg/dm³]	Stoffraum [dm³]	Festanteil [M.%]	Flüssiganteil [l]
Fließmittel	ACE 430	1,00	0,92	9,89	1,09	9,07	30,00	6,92
Konsistenzhalter	Sky 911	0,50	0,48	4,94	1,04	4,75	20,40	3,94
SRA	Rheomac 895	0,00	0,00	0,00	1,01	0,00	0,00	0,00
Beschleuniger	X-Seed	0,00	0,00	0,00	1,135	0,00	21,50	0,00
Verzögerer	Sika Tard 930	0,00	0,00	0,00	1,10	0,00	50,00	0,00
Festanteil Zusatzmittel		0,40	0,30	3,98	1,34	2,97		10,86
Wasser inkl. Flüssiganteile	Flüssigkeiten	25,00	25,00	247,20	1,00	247,20		
Zement 1	Der Violette	100,00	34,72	988,82	2,88	343,34		
Zement 2	nv	0,00	0,00	0,00	3,10	0,00		
Zusatzstoff 1 reaktiv	Elkem 940 U 20minUS	0,00	0,00	0,00	2,30	0,00		
Zusatzstoff 2 reaktiv	nv	0,00	0,00	0,00	2,50	0,00		
Zusatzstoff 3 reaktiv	nv	0,00	0,00	0,00	2,20	0,00		
Zusatzstoff 4 inert	KSM H100	10,00	3,69	98,88	2,71	36,49		
Zusatzstoff 5 inert	nv	0,00	0,00	0,00	1,06	0,00		
Zusatzstoff 6 inert	nv	0,00	0,00	0,00	1,04	0,00		
		135,40	63,71	**1338,88**	**2,13**	**630,00**		

Zuschläge

	Bezeichnung	Anteil [%]	Trocken-M. [kg]	Rohdichte tr [kg/dm³]	Stoffraum tr [dm³]	Wassergehalt [M. %]	[l]	Feucht-M. [kg/m³]
Sand 1	MEQS 0,1-0,7	100	927,5	2,65	350	0	0,00	927,50
Sand 2	nv	0	0	2,71	0	0	0,00	0,00
Sand 3	nv	0	0	2,8	0	0	0,00	0,00
***		**100**	**927,50**	**2,65**	**350,00**		**0,00**	**927,50**

Fasern

	Bezeichnung	Anteil [M.%]	Zugabe [kg/m³]	Rohdichte [kg/dm³]	Stoffraum [dm³]
Faser 1	nv	0,00	0,00	2,85	0,00
Faser 2	nv	0,00	0,00	0,91	0,00
Faser 3	nv	0,00	0,00	7,85	0,00
		0,00	**0,00**	**0,00**	**0,00**

Stoffraum

	Anteil [V. %]	Anteil [M. %]	Masse [kg]	Rohdichte [kg/dm³]	Stoffraum [dm³]
Luft	2,00	0,00	0,00	0,00	20,00
Matrix	63,00	59,08	1338,88	2,13	**630,00**
Zuschläge	35,00	40,92	927,50	2,65	350,00
Fasern	0,00	0,00	0,00	0,00	0,00
Frischbetonrohdichte			**2266,38**	4,775	1000,00
Wasserzugabe gesamt [l/m³]:			**236,35**		

Mischung

	Volumen der Mischung		2,000	dm³		V Kontrolle
	Bezeichnung	Einwaage				2000
Wasser	Wasser		472,69	g		472,69
Fließmittel	ACE 430		19,78	g		18,14
Konsistenzhalter	Sky 911		9,89	g		9,51
						0,00
						0,00
						0,00
Entlüfter	DCC-Entlüfter		2,00	g	Stoffraum nicht berücksichtigt	
Zement 1	Der Violette		1977,64	g		686,68
						0,00
						0,00
						0,00
						0,00
Zusatzstoff 4 inert	KSM H100		197,76	g		72,98
						0,00
						0,00
Sand 1	MEQS 0,1-0,7		1855,00	g		700,00
					1855,00	0,00
						0,00
						0,00
						0,00
						0,00

Mischreihenfolge und Dauer

Mischertyp:	Mischerquirl				Nachbehandlung:		
Wirblertyp:			**Wirbler**		Frischbetonprüfung Datum:		
Mischreihenfolge:	**[s]**	**[min]**	**[U/min]**	**[m/s]**	Ausbreitmaß: SFM		cm
1) Cem, MS,QM, QS, Fasern	60,0	01:00		0,0	Rohdichte:		kg/m³
2) Wasser+FM+DCC	0,0	00:00		0,0	Luftgehalt:		%
3) Mischen	120,0	02:00		0,0	Mischungstemperatur:		°C
4) Mischpause	0,0	00:00		0,0	Festbetonprüfung Datum:		
5) Mischen	0,0	00:00		0,0	Biegezug:		Mpa
6) KH einfüllen	0,0	00:00		0,0	Druck:		MPa
7) Nachmischen	0,0	00:00		0,0	Rohdichte:		kg/m³
8) Enlüften [60 mbar]	0,0	00:00		0,0			
Summe	180,0	03:00					

Fig. 4.11: Test attempt 0.8 mixture.

2. Calcined clay selection To get a better sense of how the different types of calcined clay behaved, we conducted three different spread tests for each: one with "slow," one with "medium," and one with "rapid" (see fig. 4.12). Due to the varying reactivity, we opted for a water-to-binder ratio (W/B) of 0.6 for "slow." For the other two types, "medium" and "rapid," we experimented with different levels of water addition initially. Eventually, we chose a W/B of 0.81 for "medium" and 0.86 for "rapid."

It was interesting to observe that the calcined clay appeared liquid while mixing, but when it was filled into the cone for the spread test, it immediately thickened and stopped flowing out of the container. The tests were conducted at various time intervals, immediately after mixing (0 min), and then at 10, 20, 30, 40, and 60 minutes. The procedure remained the same for each test: waiting for one minute before the test was due, then mixing for one minute and conducting the spread test. The results are visible in table 4.9.

(a) Spread test with clay "slow".

(b) Spread test with clay "medium".

Fig. 4.12: Spread test to define which of the clay we use.

time [s]	Spread Metaver N "slow" [cm] w/b=0,60	Spread Metaver I "medium" [cm] w/b=0,81	Spread Metaver O "rapid" [cm] w/b=0,86
0	9,4	9,0	9,0
10	9,4	7,8	9,1
20	7,5	8,0	9,1
30	7,4	7,5	9,5
40	7,4	7,8	10,5
60	7,5	7,8	10,0

Tab. 4.9: Clay test.

Bibliography

[1] K. Academy. *What is buoyant force?* 2023. URL: https://www.khanacademy.org/science/physics/fluids/buoyant-force-and-archimedes-principle/a/buoyant-force-and-archimedes-principle-article (visited on 07/01/2023).

[2] M. G. M. Ahmed M. Abd El-Motaal Ahmed H. Abd El-Raheem. "Effect of Time and Speed Mixes on Concrete Properties". In: *International Journal of Engineering and Innovative Technology (IJEIT)* 9 (2020). DOI: DOI:10.17605/OSF.IO/5XDK3.

[3] I. Aiad, S. Abd El-Aleem, and H. El-Didamony. "Effect of delaying addition of some concrete admixtures on the rheological properties of cement pastes". In: *Cement and Concrete Research* 32 (2002), pp. 1839–1843. ISSN: 0008-8846. DOI: https://doi.org/10.1016/S0008-8846(02)00886-4. URL: https://www.sciencedirect.com/science/article/pii/S0008884602008864.

[4] M. ANTONI. "Investigation of cement substitution by blends of calcined clays and limestone". PhD thesis. LAUSANNE: FEDERAL INSTITUTE OF TECHNOLOGY IN LAUSANNE, 2013. DOI: https://doi.org/10.5075/epfl-thesis-6001.

[5] J. J. Assaad and Y. Daou. "Cementitious grouts with adapted rheological properties for injection by vacuum techniques". In: *Cement and Concrete Research 59* (2014), pp. 43–54. DOI: https://doi.org/10.1016/S0733-5210(03)00059-6.

[6] J. F. H. Barnes H. A. and K. Walters. *An Introduction to Rheology*. 3rd ed. Netherlands: Elsevier, 1989.

[7] BerneggerGMBH. *Sicherheitsdatenblatt Kalksteinmehl*. 2023. URL: https://www.bernegger.at/images/downloads/Materialsicherheitsdatenblatt/Materialsicherheitsdatenblatt_Kalksteinmehl_V3_01_2015.pdf (visited on 07/28/2023).

[8] O. Canbek, F. Lolli, C. Childs, N. Washburn, and K. Kurtis. "Multi-Objective Design of LC3: Sustainability and Strength". In: July 2022.

[9] J. M. Crow. "The concrete conundrum". In: *Chemistry World* (2008), pp. 62–66. DOI: 10.1016/j.cemconres.2007.09.008.

[10] *DIN 4108 4:2020 11: Wärmeschutz und Energie-Einsparung in Gebäuden - Teil 4: Wärme- und feuchteschutztechnische Bemessungswerte*. Deutsch. Berlin: DIN Deutsches Institut für Normung e. V., Nov. 2020.

[11] *DIN-EN-206/1:2021-06: Beton - Festlegung, Eigenschaften, Herstellung und Konformität*. Deutsch. Wien: Austrian Standards, June 2021.

[12] B. Dženis Borovina. "Die Wirkung unterschiedlicher Fließmittel auf die Fließfähigkeit von Wasser-Pulver-Gemischen für Ressourcen-optimierten, nachhaltigen Beton". Diplomarbeit. Graz: TU Graz, 2014.

[13] EASAC. *Decarbonisation of buildings:for climate, health and jobs*. Research rep. German National Academy of Sciences Leopoldina 2021, 2021. 83 pp.

[14] Elkem. *What is silica fume?* 2023. URL: https://www.elkem.com/products/silicon/silica-fume/ (visited on 08/01/2023).

[15] S. M. Elshahawi M Hückler A. "Infra lightweight concrete: A decade of investigation (a review)." In: *Structural Concrete* 1 (2021), pp. 1–58. DOI: https://doi.org/10.1002/suco.202000206.

[16] *Eurocode 2: Bemessung und Konstruktion von Stahlbeton- und Spannbetontragwerken - Teil 1-1: Allgemeine Bemessungsregeln und Regeln für den Hochbau*. Deutsch. Wien: Austrian Standards, Jan. 2011.

[17] F. D. L. Ferraris C. and N. Martys. "Fresh Concrete Rheology: Recent Development". In: *In: Materials Science of Concrete VI* (2001), pp. 215–241.

[18] R. Flatt and I. Schober. "Superplasticizers and the rheology of concrete". In: *Understanding the Rheology of Concrete* 1 (2014), pp. 144–208. DOI: https://doi.org/10.1533/9780857095282.2.144.

[19] T. B. GMBH. *Toni Technik*. 2023. URL: https://tonitechnik.com/de/product/lastrahmen-fuer-druckfestigkeitspruefungen-bauform-2031-2/ (visited on 10/26/2023).

[20] HolcimGmbH. *PRODUKTDATENBLATT: DER BLAUE*. 2023. URL: https://www.holcim.at/fileadmin/Bibliothek/2_Zement/PDBL2023/PDBL_Der_Blaue_Mannersdorf.pdf (visited on 06/12/2023).

[21] T. H. Karl-Christian Thienel and N. beuntner. "Lightweight Concrete—From Basics to Innovations". In: *Numerical Algorithms* 3 (2020), pp. 1–5. DOI: https://doi.org/10.3390/ma13051120.

[22] LC3. *Limestone Calcined Clay Cement*. 2023. URL: https://lc3.ch/ (visited on 09/09/2023).

[23] Liapor. *Die in heller Sichtbetonoptik erstellte Gebäudehülle aus Liapor-Leichtbeton passt perfekt zum skulpturalen Charakter des Kirchenneubaus*. 2023. URL: https://www.liapor.com/bilder/lia_bilder/foto_gross/434_liapor_kirche_pliezhausen_bild1.jpg (visited on 10/10/2023).

[24] LiasÖsterreichGesmbH. *Liapor*. 2023. URL: https://www.liapor.com/at/anwendungen/hochbau.html (visited on 09/29/2023).

[25] M. I. Limited. "Understanding Yield StressMeasurements". In: (2012). URL: https://www.atascientific.com.au/wp-content/uploads/2017/02/MRK1782-01.pdf.

[26] J. Ma, M. Orgass, and N. Tue. "Influence of addition method of suplerplasticizer on the properties of fresh UHPC". In: Mar. 2008.

[27] MasterBuildersSolutions. *Technisches Merkblatt: masterGlenium ACE 430*. 2023. URL: https://www.master-builders-solutions.com/de-at/produkte/masterglenium/masterglenium-ace-430 (visited on 06/24/2023).

[28] MasterBuildersSolutions. *Technisches Merkblatt: MasterSure 930*. 2023. URL: https://www.master-builders-solutions.com/de-ch/produkte/mastersure/mastersure-930 (visited on 06/24/2023).

[29] NadhimAbdulwahidHamahSor. "The effect of superplasticizer dosage on fresh properties of selfcompacting lightweight concrete produced with coarse pumice aggregate". In: 5 (2018). DOI: https://doi.org/10.24271/garmian.336.

[30] S. Nejad Ghafar-A. Draganovic - A. Larsson. *AN EXPERIMENTAL STUDY OF THE INFLUENCE OF DYNAMIC PRESSURE ON IMPROVING GROUT PENETRABILITY*. Research rep. ROCK ENGINEERING RESEARCH FOUNDATION STIFTELSEN BERGTEKNISK FORSKNING, 2015. 96 pp.

[31] NEWCHEMGmbH. *Technical data sheet Metaver n.* URL: http://catalogue.newchem.org/Uploads/637029666293025241MDS%20Metaver%20N%202019%20en.pdf (visited on 05/14/2023).

[32] *ÖNORM B 4710-2:2020 03 01: Beton - Festlegung, Eigenschaften, Herstellung, Verwendung und Konformität - Teil 2: Regeln zur Umsetzung der ÖNORM EN 206 für gefügedichten Leichtbeton mit einer Trockenrohdichte von 800 kg/m³ bis 2 000 kg/m³*. Deutsch. Wien: Austrian Standards, Mar. 2020.

[33] *ÖNORM EN 1097-6-1:2022-02: Prüfverfahren für mechanische und physikalische Eigenschaften von Gesteinskörnungen — Teil 6: Bestimmung der Rohdichte und der Wasseraufnahme*. Deutsch. Wien: Austrian Standards, Feb. 2022.

[34] L. Pointner. "Infiltration of cement paste in porous media". Diplomarbeit. Wien: TU Wien, 2021. DOI: 10.34726/hss.2021.64286.

[35] PRASAD. *Lightweight Concrete types and properties*. 2023. URL: https://www.structuralguide.com/lightweight-concrete/ (visited on 02/23/2023).

[36] M. Ramizi. "Concept development for the design of a permeable paving stone". Diplomarbeit. Wien: TU Wien, 2022. DOI: 10.34726/hss.2022.90834.

[37] T. Reschke. *12. Der Einfluss der Granulometrie der Feinstoffe auf die Gefügeentwicklung und die Festigkeit von Beton*. Düsseldorf: Verlag Bau+Technik, 2001. ISBN: 978-3-764-00406-4.

[38] C. M. Richard P. "Composition of reactive powder concretes". In: *Cement and Concrete Research* 25.7 (1995), pp. 1501–1511. ISSN: 0008-8846. DOI: https://doi.org/10.1016/0008-8846(95)00144-2.

[39] L. S.P.A. *Technical-data-sheet-Laterlite-Expanded-Clay*. 2023. URL: https://www.laterlite.com/wp-content/uploads/2022/05/Technical-data-sheet-Laterlite-Expanded-Clay.pdf (visited on 01/18/2023).

[40] J. Schindelin, I. Arganda-Carreras, A. Cardona, M. Longair, B. Schmid, et al. *Fiji Imagej*. 2022. URL: https://imagej.net/software/fiji/ (visited on 08/05/2023).

[41] K. Scrivener, F. Martirena, S. Bishnoi, and S. Maity. "Calcined clay limestone cements (LC3)". In: *Cement and Concrete Research* 114 (2018), pp. 49–56. ISSN: 0008-8846. DOI: https://doi.org/10.1016/j.cemconres.2017.08.017. URL: https://www.sciencedirect.com/science/article/pii/S0008884617302454.

[42] T.Liberto. "Werkstoffe im Bauwesen Laborübung". In: *Frisch- und Festbeton* (2020).

[43] *Thermalconductivity*. 2023. URL: https://en.wikipedia.org/wiki/Thermal_conductivity (visited on 08/10/2023).

[44] U.-P. D.-I. K.-C. Thienel. *Gefügedichter und haufwerksporiger Leichtbeton*. Research rep. Universität der Bundeswehr München, 2018. 36 pp.

[45] H. H. Wong and A. K. Kwan. "Packing density of cementitious materials: Measurement and modelling". In: *Magazine of Concrete Research 60* (2008), pp. 165–175. DOI: 10.1680/macr.2007.00004.

List of Figures

List of Tables